

# Weakly non-linear analysis of wind-driven gravity waves

By **Alexandros Alexakis**<sup>1</sup>, **Yuan-Nan Young**<sup>2</sup> and **Robert Rosner**<sup>3</sup>

<sup>1</sup> Department of Physics, University of Chicago, Chicago, IL 60637, USA

<sup>2</sup> Department of Engineering Sciences & Applied Mathematics, Northwestern University, Evanston, IL, 60208, USA

<sup>3</sup> Departments of Physics and of Astronomy & Astrophysics, University of Chicago, Chicago, IL 60637, USA

(Received 5th November 2018)

We study the weakly non-linear development of shear-driven gravity waves, following the physical mechanism first proposed by Miles and furthermore investigate the mixing properties of the finite amplitude solutions. Calculations to date have been restricted to the linear theory, which predicts that gravity waves are amplified by an influx of energy through the critical layer, where the velocity of the wind equals the wave phase velocity. Because of the presence of a critical layer, ordinary weakly non-linear methods fail; in this paper, we use a rescaling at the critical layer and matched asymptotics to derive an amplitude equation for the most unstable wave, under the simplifying assumption that the physical domain is periodic. These amplitude equations are solved numerically, in their quasi-steady limit, for the cases of small density ratio (applicable to oceanography), and for arbitrary density ratio but strong stratification (for more general physical/astrophysical situations). As is found in other analysis for critical layers in inviscid parallel flow, we find that the initial exponential increase of the amplitude  $A$  transitions to an algebraic growth rate proportional to the viscosity,  $A \sim \nu t^{2/3}$ . However, for the air over water case (provided the maximum wind velocity is in the range of  $0.2 \text{ m s}^{-1} \sim 1 \text{ m s}^{-1}$ ), our results from the weakly non-linear analysis for the single mode show that the transition from exponential to algebraic growth rate occurs when the amplitude of the wave is as small as  $h \sim 10^{-5} \lambda$ ; hence, it may be difficult to observe the linear regime for this case in numerical simulations. (Whether this result transfers to cases in which the physical domain is not periodic, so that the marginally stable modes form a continuum, is not as yet known.) We also find that the weakly non-linear flow allows for super-diffusive particle transport with an exponent  $\sim 3/2$ , consistent with Venkataramani's results.

## 1. Introduction

The generation of surface waves by winds has been a problem under study for well over a century. The simple model of Kelvin-Helmholtz (from now on, KH) instability provided higher bounds on the maximum wind velocity for the instability to occur than what was experimentally observed (Chandrasekhar (1961), §101); and a solution was not available until Miles (1957, 1959*a,b*, 1962, 1967) proposed a model in which gravity ocean waves are amplified through a ‘resonant’ interaction with the wind above the ocean surface: Waves that travel with speed  $c = \sqrt{g/k}$  are amplified through an influx of energy at the height  $y_c$  in the wind where the wind speed  $U(y)$  matches the wave speed,  $U(y = y_c) = c$ . Miles explicitly assumed that the wind profile above the sea surface was of the form  $\log(z/z^*)$  (where  $z^*$  is a parameter), composed of a mean velocity  $U$  and a turbulent component  $u$ . Assuming the mean wind profile to be given from turbulent boundary layer theory and the turbulent component to be small, he calculated the influx of energy to the wave. This analysis involved the treatment of the critical layer (the point where the velocity of the wind was equal to the velocity of the gravity wave), where the solution of the linear eigenfunction problem becomes singular (the  $x$ -component of the perturbation velocity behaves as  $u \sim \log(y - y_c)$ ). The singularity is removed either because there is an imaginary component of  $c$  (i.e., unsteady critical layer) or because viscosity becomes important in this thin layer (i.e., viscous critical layer). In both cases, the final result is that there is an ‘ $-i\pi$  phase change’ across the critical layer, e.g., the perturbation wave above the critical layer is not in phase with the wave below. A direct result of this phase change is that the gravity wave will become unstable because a component of the pressure perturbation will be in phase with the slope of the wave (unlike the KH case, in which the pressure perturbation wave is always in phase with the wave). Using the results from linear theory and for small density ratios, Miles predicted the energy flux from the wind to the gravity wave.

Our interest in this problem is motivated by an astrophysical puzzle, namely, the mixing of carbon/oxygen (C/O) at the surface of a white dwarf with accreted material (mostly hydrogen and helium, He/H) overlying the stellar surface (whose presumed origin is from an accretion disk surrounding the compact star). For a variety of reasons, it is thought that the accreted envelope is in differential rotation with respect to the stellar surface, so that a ‘wind’ is expected at this surface (Rosner, Alexakis, Young & Truran, Hillebrandt 2001). In this stellar case, one is forced to generalize the earlier results to arbitrary density ratios (between the ‘atmosphere’ and the ‘surface material’); and we have already done so for the linear problem (Alexakis, Young & Rosner 2002), deriving bounds on the instability in the parameter space, and estimating the growth rates of the unstable modes. While useful as a starting point for further analysis, linear theory gives no information about the ultimate fate of the system, which is largely governed by nonlinear processes. In this paper, we uncover the non-linear effects on the evolution of wind-driven surface waves by examining their finite-amplitude evolution. To explore the applications to the relevant astrophysical and geophysical systems, we also investigate the mixing property of the weakly non-linear flow using particle method, and results show enhanced mixing due to the coupling of the weakly nonlinear wind with the surface wave.

We note here that the weakly non-linear theory for the KH instability has already been derived by Drazin (1970). That analysis cannot be applied straightforwardly to our problem because of the presence of critical layers: Due to the singularity that appear in the linear theory at the point where the phase speed of a surface wave matches the wind speed, higher order terms in the expansion become more singular and the expansion must

ultimately fail. The fundamental reason for this behavior is that the flow becomes non-linear first inside the critical layer even though the rest of the flow can still be considered as operating in the linear regime. For this reason, a more refined treatment of the critical layer is required. The necessary analytical ‘machinery’ fortunately already exists: Thus, Benney & Bergon (1969), and later Benney & Maslowe (1975), observed that for small but finite amplitudes the phase change at the critical layer does not necessarily have to be  $-i\pi$ ; instead, they found a solution with the property that if the nonlinear terms are taken into account, the phase change is zero. Later Haberman (1972) showed numerically that there is a smooth increase of the phase change, from  $-i\pi$  to 0, and introduced the function  $\Phi$  that gives the phase change as a function of the amplitude; Churilov & Shukman (1987, 1988, 1996) then developed a weakly nonlinear theory based on  $\Phi$  and other similar functions defined for the appropriate critical layer problem. A fundamental assumption in all this work is that the viscosity is dominant in the critical layer; this leads to the derivation of an ordinary differential equation for the wave amplitude. The full equations of the weakly nonlinear problem without making the previous assumption have then been solved numerically for various cases (Goldstein & Hultgen 1988; Warn & Warn 1978; Balmforth & Piccolo 2001).

In our case the treatment – although closely related to the earlier work – is nevertheless different in two respects. The first one is that the previous cases possess stability boundaries for modes for which the critical layer is formed at the inflection point  $\partial_y^2 U / \partial y^2 = 0$ ; one then examines the close-to-marginally-stable state unstable modes. This is however not our case since such an inflection point does not exist (unless one considers  $U(\infty)$  as such a point). Instead, we will be considering two special cases: the case of small density ratio, and the case of very strong stratification<sup>†</sup>; in both cases, the linear growth rate is small. This procedure will lead to a slightly different scaling. The second difference lies in the fact that we have an interface. Because of this, our solvability condition will not be expressed in terms of integrals but rather in terms of appropriate vector products of the values of the perturbation stream function at the interface.

This paper is structured as follows. First we formulate our problem and describe the non-dimensionalized form of the basic problem equations. In §3 we very briefly review (and slightly revise) the linear theory developed earlier (Alexakis, Young & Rosner 2002). The amplitude equations are derived in §4.1 and §4.2 for the small density ratio and the strongly stratified cases, respectively (we define these terms more precisely in what follows). We summarize the conservation laws from the amplitude equations in §5.1, and we discuss the implications of the long-time behavior of surface waves in §5.2. In §5.3 we summarize results from numerically simulating the amplitude equations. In §6 we investigate how the coupling between the wind and the surface wave affects mixing properties of the finite amplitude solution. A detailed examination of the assumptions made in the analysis is provided in §7, where we also draw conclusions from our work.

## 2. Formulation

We consider a two-layer system with constant fluid density  $\rho_1$  and  $\rho_2$  ( $\rho_1 \leq \rho_2$ ), respectively, in the upper and lower layers. The interface between the two layers is given by  $y = h(x, t)$ , where  $x$  is the horizontal and  $y$  is the vertical coordinate. In the upper layer we assume a wind parallel to the originally flat interface  $y = h(x, t = 0) = 0$ . The

<sup>†</sup> This case is of particular interest to our astrophysical problem, since the instability takes place on the surface of a white dwarf star, i.e., a star of solar mass, but comparable in size to the Earth.

wind has a shear velocity profile  $\vec{U} \equiv [U(y), 0]$ , where  $U(y)$  varies only with  $y$ . The lower layer is initially at rest. Our aim is to study the dynamics and the weakly nonlinear development of a small sinusoidal perturbations of the horizontal interface.‡

The fluid is assumed incompressible in both layers; we therefore work with the stream function  $\Psi$ , which is connected to the velocity by the relation  $(u, v) = (\partial_y \Psi, -\partial_x \Psi)$ . The stream function can be separated into its mean and its perturbation components,

$$\Psi_{\text{total}} = \int_0^y U dy' + \Psi. \quad (2.1)$$

The fluid within each layer is described by the Navier-Stokes equations (in terms of the stream function  $\Psi$ ):

$$\nabla^2 \Psi_{,t} + U \nabla^2 \Psi_{,x} - U_{,yy} \Psi_{,x} = \Psi_{,x} \nabla^2 \Psi_{,y} - \Psi_{,y} \nabla^2 \Psi_{,x} + \nu \nabla^2 \nabla^2 \Psi, \quad (2.2)$$

where  $\nabla$  is the two-dimensional Laplacian and  $\nu$  is the viscosity (which we will consider to be small, and therefore negligible except for a narrow region within the critical layer). Here we have used the standard notational device of comma-prefaced subscripts to denote partial derivatives, e.g.,

$$f_{,x} \equiv \partial f / \partial x.$$

The boundary conditions at the interface are the continuity of the perpendicular component of the velocity to the interface

$$h_{,t} + (U^\pm + \Psi_{,y}^\pm) h_{,x} + \Psi_{,x}^\pm = 0, \quad (2.3)$$

and the continuity of pressure

$$\begin{aligned} \Delta \left[ \rho_i \{ \Psi_{,ty} + (U + \Psi_{,y}) \Psi_{,xy} - \Psi_{,x} (U_{,y} + \Psi_{,yy}) - h_{,x} (\Psi_{,tx} + (U + \Psi_{,y}) \Psi_{,xx} + \Psi_{,x} \Psi_{,xy}) \} \right] \\ = g h_{,x} (\rho_2 - \rho_1), \end{aligned} \quad (2.4)$$

where  $h(x)$  is the elevation of the interface and all quantities above are evaluated at  $y = h(x)$ . The  $\pm$  indices indicate values above and below the interface, and  $\Delta[ \ ]$  denotes the difference across  $y = h$  (e.g.,  $\Delta[f(y)] = f(h^+) - f(h^-)$ ).

We non-dimensionalize lengths by the characteristic length  $l$  of the wind, and velocities by the asymptotic value of the wind at  $y \rightarrow +\infty$ ,  $U_{max}$ . An important parameter that emerges from the scaling is  $G \equiv gl/U^2$ , which is a measure of the ratio of potential energy to kinetic energy, or alternatively, a measure of the strength of the stratification. Other dimensionless parameters are the Reynolds number,  $Re \equiv Ul/\nu \gg 1$ , and the ratio of densities,  $r \equiv \rho_1/\rho_2 \leq 1$ . In terms of the non-dimensional parameters, we focus on cases

‡ As an aside, we note that the presence of a sharp interface boundary between the two fluids in our system is really only a device to simplify the analysis, but in no way restricts our results. That is, in a more general case there will be no sharp interface, but the density will change smoothly from  $\rho_2$  to  $\rho_1$  in a layer of width  $\delta_1$ . We would then also expect  $U(y)$  to be a smooth function in  $y$ , so that any flow discontinuity at the interface would be replaced by a smooth variation in  $U$  within a thin viscous boundary layer of width  $\delta_2$ . One would then expect to see differences in behavior only for those modes with horizontal wavenumber  $k$  large enough so that the critical layer lies inside these layers  $\delta_1, \delta_2$ . Such modes, however, are KH-modes which are not under study here; they will obey a Richardson-type stability criterion,  $1/4 < g(\Delta\rho/\rho)\delta_2^2/\delta_1$  (Chandrasekhar 1961). We therefore expect our assumption of a sharp interface to be reasonable for horizontal wave-numbers  $k^{-1} \geq \max\{\delta_1, \delta_2\}$ . Since we are primarily interested in long wavelength perturbations, we conclude that, for our purposes, we have not disregarded any important physics.

where  $Re \gg 1$  in each layer, and especially the two distinguished limits  $r \ll 1$  (air on water, for example) and arbitrary ‘large’ density ratio  $r$  with  $G \gg 1$  (accretion on white dwarfs in astrophysics).

### 3. Linear Theory

We linearize equations (2.2) - (2.4), and write the stream function perturbation  $\Psi$  and surface elevation  $h$  as a traveling wave parallel to the wind (right traveling wave in our setup)

$$\begin{aligned}\Psi^\pm(y, x, t) &= \phi^\pm(y)e^{iK(x-Ct)} + \text{c.c.}, \\ h &= \tilde{h}e^{iK(x-Ct)} + \text{c.c.},\end{aligned}$$

where c.c. denotes the complex conjugate, and  $K = kl$  is the non-dimensional (horizontal) wavenumber and  $C$  is the non-dimensional phase velocity. This leads us to the well-studied Rayleigh equation (Drazin & Reid 1981)

$$\phi_{,yy}^\pm - \left[ K^2 + \frac{U_{,yy}}{U-C} \right] \phi^\pm = 0, \quad (3.1)$$

where the inviscid limit  $Re \rightarrow \infty$  is taken. The boundary conditions become

$$(U^\pm - C)\tilde{h} + \phi^\pm = 0, \quad (3.2)$$

$$\Delta[\rho_i((U^\pm - C)\phi_{,y} - U_{,y}^\pm\phi^\pm)] - G\tilde{h}(\rho_2 - \rho_1) = 0, \quad (3.3)$$

Eliminating  $\phi^-$  and  $\tilde{h}$  from the last two equations, and dropping the + index for convenience, we obtain

$$KC^2 - r \left[ (U-C)^2\phi_{,y} - (U-C)U_{,y} \right] - G(1-r) = 0, \quad (3.4)$$

where we have used  $\phi^+|_{y=0} = 1$  as a normalization condition.

To further simplify we assume that  $U(0) = 0$  and omit the KH-modes (of which the nonlinear evolution is not under study here, see Alexakis, Young & Rosner (2002) for more details). The linear growth rate ( $K\text{Im}(C)$ ) has been numerically calculated and summarized in Alexakis, Young & Rosner (2002) for cases of interests. Here we briefly summarize some relevant results on stability boundaries for the wind profile

$$U = 1 - e^{-y}. \quad (3.5)$$

As shown in Alexakis, Young & Rosner (2002), this wind profile allows for an analytic expression for the stability boundaries in the stability diagram. One can show that some general features of the stability boundaries summarized here for wind profile in equation (3.5) also hold for other bounded wind profiles. The stability bound comes from the modes that have phase velocity  $C = 1$ , in which case the solution of equation (3.1) becomes  $\phi = e^{i\kappa x}$  with  $\kappa = \sqrt{1 + K^2}$ . Applying the boundary conditions, one obtains the criterion on wavenumber  $K$  for the unstable modes:

$$K \geq K_{min} = \frac{G(1-r) + r - r\sqrt{(G(1-r) + r)^2 + (1-r^2)}}{1-r^2}. \quad (3.6)$$

The unstable modes can be further restricted if we assume the presence of surface tension or magnetic fields. This will lead to an additional term  $\mathcal{T}K^2$  in equation (3.4), where

$\mathcal{T} = \sigma/(\rho_2 U_{max}^2 l)$  and  $\sigma$  is the surface tension<sup>†</sup>. Then the unstable modes lie in the region  $K_{min} \leq K \leq K_{max}$ , where  $K_{min}$  and  $K_{max}$  are given by the positive real solutions of

$$K + r\sqrt{1 + K^2} - (G(1 - r) + r + \mathcal{T}(K)K^2) = 0. \quad (3.7)$$

Furthermore, there is a minimum value of  $\mathcal{T}$  below which the above equation has no positive real solutions, and therefore no unstable modes exist. The physics behind these bounds is simple: In order for a mode to become unstable for the above wind profile, the phase velocity of the wave must lie in the range  $0 < c < U_{max}$  (Alexakis, Young & Rosner 2002). With the inclusion of surface tension, the phase velocity is not monotonic with  $K$ , but for large enough  $K$ , the phase velocity increases in an unbounded fashion. This leaves only a finite region in  $K$  space with phase velocity smaller than  $U_{max}$ ; moreover, if the surface tension is large enough, the minimum phase velocity is larger than  $U_{max}$ , and therefore no unstable mode exists.

The analysis is simplified if we assume small density ratio, and expand all quantities in  $r$ :

$$\begin{aligned} C &= C_0 + rC_1 + \dots \\ \phi &= \phi_0 + r\phi_1 + \dots \end{aligned}$$

In that case the linear theory, to zero order, gives a gravity wave with phase velocity  $C_0 = \sqrt{G/K}$ . At the next order, one obtains

$$2C_0C_1 = [C_0^2\phi_{0,y} + U_{,y}] - G, \quad (3.8)$$

and therefore

$$\text{Im}\{C_1\} = \frac{1}{2}C\text{Im}\{\phi_{0,y}\} \quad (3.9)$$

where  $\phi_0$  is such that

$$\phi_{0,yy} - \left[ K^2 + \frac{U_{,yy}}{U - C_0} \right] \phi_0 = 0. \quad (3.10)$$

An  $-i\pi$  phase change at the critical level is assumed. Due to this phase change,  $\phi_{0,y}$  is complex at the interface and thus  $C_1$  has an imaginary component, which is responsible for the instability of the traveling waves.

For the arbitrary  $r$  case, the previous expansion does not hold, and one needs to solve the full set of equations (3.1)-(3.4) as in Alexakis, Young & Rosner (2002). There it was shown that the growth rate exhibits an exponential dependence on the parameter  $G$ . In Appendix A, we carry out an asymptotic analysis for large  $G$ , and derive this exponential dependence. More specifically, the growth rate is found to be

$$K \text{ Im}\{C\} = \frac{r\pi^2}{4(1-r)} \frac{1}{\mathcal{A}_t G} \left( \frac{\mathcal{A}_t G}{K} \right)^{3/2} \left[ \left( 1 - \frac{1}{\sqrt{K/(\mathcal{A}_t G)}} \right)^{(K/\mathcal{A}_t G)} \right]^{2\mathcal{A}_t G}, \quad (3.11)$$

where  $\mathcal{A}_t$  is the Atwood number. As is shown in the Appendix, the stream function  $\Psi$  below the critical layer is composed of an exponentially increasing and an exponentially decreasing component. Since the boundary condition (equation (3.2)) must be satisfied, the exponentially large component must be in phase with  $h$ , which leaves us with the exponentially small, out of phase, component to drive the wave unstable. A detailed calculation then leads to the result given above.

<sup>†</sup> We note that a magnetic field whose direction is aligned with the interface will have the same effect as surface tension with  $\sigma(K) = B^2/(2\pi\mu K)$  (Chandrasekhar 1961).

#### 4. Weakly nonlinear theory

We are now ready to embark upon the weakly non-linear theory. Formally this is done by assuming that, for some parameter ranges of interests, our physical system lies close to a marginally stable state so that an asymptotic expansion is allowed near the center manifold. For the problem at hand, however, and in the absence of surface tension ( $\mathcal{T} = 0$ ), marginally stable states are possible only when  $r = 0$  or  $1/G = 0$  (we note that  $K$  is not a control parameter); the first one expresses the unphysical situation that there is no upper fluid, and the latter corresponds to a situation where there is no wind in the upper fluid ( $U \sim 1/\sqrt{G}$ ). Complication arises as we deviate from these neutrally stable states. In ordinary dissipative systems, only a small number of modes near the center manifold become unstable and need to be considered. In our case though, once the density ratio  $r$  or the parameter  $G$  is finite, an infinite number of modes become unstable if surface tension  $\mathcal{T} = 0$ . Ideally the interaction of all these modes needs to be taken into account. Practically this difficulty is removed by the combined effect of surface tension  $\mathcal{T}$  (or, equivalently, the presence of a magnetic field) and weak viscous damping. In the presence of surface tension the stability boundary in the  $(r, G, \mathcal{T})$  space is given by the condition for positive solutions of eq.(3.7) for  $r = 0$ . Surface tension reduces the number of unstable modes by neutralizing modes of wave numbers above some cut-off value. Further more weak viscosity will damp out the neutrally stable modes of high wave numbers, rendering them asymptotically stable. Using a periodic domain we can always fix the period so that only one mode becomes unstable. We can then derive the amplitude equation for this single mode as usual.

We find that these amplitude equations are almost the same as those obtained from asymptotic expansion around the most unstable mode without surface tension; the only difference is a coefficient dependence on the surface tension. In the following derivation, for simplicity, we chose not to include surface tension, and assume the presence of surface tension only implicitly. At the end of the analysis the surface tension can always be recovered by replacing  $G$  with  $G + \mathcal{T}K^2$ .

With the previously stated assumptions, and following the basic strategy of the weakly nonlinear theory, we develop below an asymptotic expansion based on the small amplitude of the perturbation, and introduce a long time scale of the same order as the nonlinear terms inside the critical layer. We consider two different cases: The first case assumes that the density ratio is small ( $r \ll 1$ ); the second case allows for arbitrary  $r$  but assumes that  $G \gg 1$ . The small density ratio ( $r$ ) in the first case is the parameter to which we scale our amplitudes. The large  $G$  and arbitrary  $r$  case, however, is a bit more complicated; for this case, the growth rate according to linear theory is proportional to  $\exp(-2G)$ , and this will be our scaling parameter.

##### 4.1. Small density ratio case

We start with the small  $r$  case. The following analysis applies to for a monotonically increasing but otherwise arbitrary wind-profile. The outline of the derivation is as follows: we write the Euler equations, and the boundary conditions, in the reference frame of the moving wave. We introduce the scaling discussed below, and solve up to the second order; this requires a more detailed treatment at the critical layer that determines the phase change across the layer. Using matched asymptotics, we match the inner solution with the Frobenius solutions  $\phi_a, \phi_b$  of the outer flow. This introduces five different amplitudes,  $A_1^\pm, B_1^\pm$ , and  $A_2$ , for each Frobenius solution above and below the critical layer (which will be assumed to be given numerically); the fifth amplitude  $A_2$  is just the surface wave amplitude. The first four amplitudes are connected through the boundary conditions at infinity and the matching at the critical layer; the fifth is connected with the rest through

the boundary conditions at the interface. When we apply the boundary conditions, the first order gives the free gravity wave (vacuum over water); at second order, the solvability condition results in the amplitude equation.

We begin by introducing the scaling. Let  $\epsilon \equiv \rho_1/\rho_2 \ll 1$  and  $\partial_t \equiv \epsilon \partial_T - C \partial_x$ . Then the equation for the stream function in the reference frame of the wave will be:

$$\epsilon \nabla^2 \Psi_{,T} + (U - C) \nabla^2 \Psi_{,x} - U_{,yy} \Psi_{,x} = \Psi_{,x} \nabla^2 \Psi_{,y} - \Psi_{,y} \nabla^2 \Psi_{,x} + \frac{1}{R} \nabla^2 \nabla^2 \Psi, \quad (4.1)$$

with boundary conditions at  $y = 0$

$$\epsilon h_{,T} - C h_{,x} + \Psi_{,x}^{\pm} = \text{non-linear terms} \quad (4.2)$$

and

$$\epsilon \left[ \epsilon \Psi_{,Ty}^+ - C \Psi_{,xy}^+ - U_{,y}^+ \Psi_{,x}^+ \right] - \left[ \Psi_{,Ty}^- C \Psi_{,xy}^- - U_{,y}^- \Psi_{,x}^- \right] - G h_{,x} (1 - \epsilon) = \text{non-linear terms}, \quad (4.3)$$

where the  $\pm$  index means above or below the interface. First we focus on the upper fluid and the outer solution (outside the critical layer).

#### 4.1.1. Outer solution in upper fluid

We expand the stream function as

$$\Psi = \epsilon^2 \Psi_0 + \epsilon^3 \Psi_1 + \dots \quad (4.4)$$

To zeroth order we have

$$(U - C) \nabla^2 \Psi_{0,x} - U_{,yy} \Psi_{0,x} = 0.$$

Focusing on the most unstable mode and writing  $\Psi_0 = A(T) \phi(y) e^{iKx} + \text{c.c.}$ , we obtain:

$$\phi_{,y} - \left[ K^2 + \frac{U_{,yy}}{U - C} \right] \phi = 0.$$

Near the critical layer  $y \rightarrow y_c$  the solution can be written as

$$\phi = a^{\pm} \phi_a + b^{\pm} \phi_b.$$

The  $\pm$  signs correspond to above or below the critical layer, and the two Frobenius solutions are

$$\phi_a = \left( 1 + \frac{U_c''}{U_c'} (y - y_c) \ln |y - y_c| + \dots \right), \quad (4.5)$$

$$\phi_b = \left( \frac{U_c''}{U_c'} (y - y_c) + \dots \right), \quad (4.6)$$

where  $U_c'$  and  $U_c''$  are  $\partial U / \partial y|_{y=y_c}$  and  $\partial^2 U / \partial y^2|_{y=y_c}$ , respectively. In general,  $a^{\pm}$  and  $b^{\pm}$  are functions of  $T$ , so that it is more convenient to write the solution as

$$\Psi_0 = [A_{1\pm}(T) \phi_a(y) + B_{1\pm}(T) \phi_b(y)] e^{iKx} + \text{c.c.} \quad (4.7)$$

At the next order, we have

$$(U - C) \nabla^2 \Psi_{1,x} - U_{,yy} \Psi_1 = -\nabla^2 \Psi_{0,T}.$$

Again expanding  $\Psi_1$  in terms of Frobenius solutions, we write  $\Psi_1$  as

$$\Psi_1 = \left( \hat{A}_{1\pm} \phi_a + \hat{B}_{1\pm} \phi_b + A_{1\pm,T} \frac{U_c''}{U_c'^2} \ln |y| + \dots \right) e^{iKx} + \text{c.c.},$$

where  $\hat{A}_{1\pm}$  and  $\hat{B}_{1\pm}$  are the amplitudes of  $\Psi_1$ . In order to match with the inner solution, we require the behavior of  $\Psi$  as  $(y - y_c) \rightarrow \epsilon Y$ . Upon expansion in  $Y$  we obtain

$$\begin{aligned} \Psi &= \epsilon^2 \Psi_0 + \epsilon^3 \Psi_1 + \dots \\ &= \left\{ \epsilon^2 A_{1\pm} + \epsilon^3 \ln(\epsilon) \left[ A_{1\pm} \frac{U_c''}{U_c'} Y + \partial_T A_{1\pm} \frac{U_c''}{U_c'^2} \right] + \right. \\ &\quad \left. + \epsilon^3 \left[ B_{1\pm} \frac{U_c''}{U_c'} Y + A_{1\pm} \frac{U_c''}{U_c'} Y \ln |Y| + \partial_T A_{1\pm} \frac{U_c''}{U_c'^2} \ln |Y| \right] + \dots \right\} e^{iKx} + \text{c.c.} \end{aligned}$$

#### 4.1.2. Inner solution

To capture the dynamics inside the critical layer, we have to use the scaling  $\Psi \rightarrow \epsilon^2 \tilde{\Psi}(Y)$ ,  $y - y_c \rightarrow \epsilon Y$  and  $1/R \rightarrow \epsilon^3 \nu$ . From equation (4.1) we then obtain

$$\begin{aligned} \tilde{\Psi}_{,TTY} + U_c' Y \tilde{\Psi}_{,xYY} + \tilde{\Psi}_{,Y} \tilde{\Psi}_{,YYx} - \tilde{\Psi}_{,x} \tilde{\Psi}_{,YYY} - \nu \tilde{\Psi}_{,YYY} \\ = -\epsilon \left[ \frac{1}{2} U_c'' Y^2 \tilde{\Psi}_{,YYx} - U_c'' \tilde{\Psi}_{,x} \right] + \mathcal{O}(\epsilon^2). \end{aligned} \quad (4.8)$$

In order to match with the outer solution we expand  $\tilde{\Psi}$  as

$$\tilde{\Psi} = \tilde{\Psi}_0 + \epsilon \ln(\epsilon) \tilde{\Psi}_1 + \epsilon \tilde{\Psi}_2 + \epsilon^2 \ln(\epsilon) \tilde{\Psi}_3 + \epsilon^2 \tilde{\Psi}_4 + \dots$$

To first order, we then have

$$\tilde{\Psi}_{0,TTY} + U_c' Y \tilde{\Psi}_{0,xYY} + \tilde{\Psi}_{0,Y} \tilde{\Psi}_{0,YYx} - \tilde{\Psi}_{0,x} \tilde{\Psi}_{0,YYY} - \nu \tilde{\Psi}_{0,YYY} = 0.$$

Matching with the outer solution we obtain

$$\tilde{\Psi}_0 = A_{1+} e^{iKx} + A_{1+}^* e^{-iKx}, \quad (4.9)$$

and therefore

$$A_{1+} = A_{1-} = A_1. \quad (4.10)$$

To second order ( $\epsilon \ln(\epsilon)$ ), we have

$$\tilde{\Psi}_{1,TTY} + U_c' Y \tilde{\Psi}_{1,xYY} - \tilde{\Psi}_{0,x} \tilde{\Psi}_{1,YYY} - \nu \tilde{\Psi}_{1,YYY} = 0.$$

Matching with the outer solution we obtain

$$\tilde{\Psi}_1 = \left[ A_1 \frac{U_c''}{U_c'} Y + \partial_T A_1 \frac{U_c''}{U_c'^2} \right] e^{iKx} + \text{c.c.} \quad (4.11)$$

To third order ( $\epsilon^3$ ), we have

$$\tilde{\Psi}_{2,YYT} + U_c' Y \tilde{\Psi}_{2,YYx} - \tilde{\Psi}_{0,x} \tilde{\Psi}_{2,YYY} - \nu \tilde{\Psi}_{2,YYY} = U_c'' \tilde{\Psi}_{0x}. \quad (4.12)$$

Denoting  $Z = \tilde{\Psi}_{2,YY}$ , which is the vorticity inside the critical layer, we obtain

$$Z_{,T} + U_c' Y Z_{,x} - \tilde{\Psi}_{0,x} Z_{,Y} - \nu Z_{,YY} = U_c'' \tilde{\Psi}_{0x}. \quad (4.13)$$

To match with the outer solution, we require the boundary conditions of  $Z$

$$\lim_{Y \rightarrow \infty} Z = \left[ A_1 \frac{U_c''}{U_c'} \frac{1}{Y} - \frac{U_c''}{U_c'^2} \frac{1}{Y^2} A_{1T} \right] e^{iKx} + \text{c.c.}$$

$$\lim_{Y \pm \infty} \Psi_{2,Y} = e^{iKx} \left[ A_1 \frac{U_c''}{U_c'} (\ln |y| + 1) + A_{1T} \frac{U_c''}{U_c'} \frac{1}{Y} + B_{1\pm} \frac{U_c''}{U_c'} \right] + \text{c.c.}$$

Integrating  $Z$  along  $Y$ , we obtain

$$\int_{-\infty}^{+\infty} Z dY = \left[ \Psi_{2,Y} \right]_{-\infty}^{+\infty} = \frac{U_c''}{U_c'} [B_{1+} - B_{1-}] e^{iKx} + \text{c.c.},$$

where in the above integral we assumed the limiting procedure  $\lim_{\epsilon \rightarrow 0} \int_{-1/\epsilon}^{1/\epsilon} Z dY$ . Let

$$J = \frac{K}{2\pi} \frac{U_c'}{U_c''} \int_{-\pi/K}^{+\pi/K} e^{-iKx} \int_{-\infty}^{+\infty} Z dY dx = B_{1+} - B_{1-}. \quad (4.14)$$

This leads to the important result:

$$B_{1-} = B_{1+} - J. \quad (4.15)$$

The last equation (4.15) implies that the phase change across the critical layer depends on the more detailed treatment of the vorticity dynamics inside the critical layer. In the linear case  $J = +i\pi A_1$ , but as the amplitude grows and the non-linear term  $\tilde{\Psi}_{0,x} Z_Y$  in equation (4.13) becomes important, the phase change is going to decrease.

#### 4.1.3. Lower fluid

Using the same scaling as for the outer solution of the upper fluid, we have

$$\Psi^- = \epsilon^2 \Psi_0^- + \epsilon^3 \Psi_1^- + \dots$$

To first order, we then have

$$\begin{aligned} \nabla^2 \Psi_x^- &= 0, \\ \Psi^- &= A_2(T) \tilde{\phi}_0^- e^{iKx+Ky} + \text{c.c.} \end{aligned}$$

At next order,

$$\begin{aligned} \nabla^2 \Psi_{0,T} - C \nabla^2 \Psi_{1,x} &= 0, \\ \Psi_1^- &= A_2'(T) \tilde{\phi}_1^- e^{iKx+Ky} + \text{c.c.} \end{aligned}$$

At this point we are ready to apply the boundary conditions at the interface, and obtain the amplitude equation.

#### 4.1.4. Boundary conditions and the amplitude equation

First, we expand the amplitude of the perturbed interface

$$h = \epsilon^2 h_0 + \epsilon^3 h_1 + \dots$$

To first order, we obtain

$$h_0 = A_2 \tilde{h}_0 e^{iKx} + \text{c.c.}$$

Then using equations (4.2) and (4.3), we obtain

$$\tilde{\phi}_0^- - C \tilde{h}_0 = 0, \quad (4.16)$$

$$-C\tilde{\phi}_0^- + G/K\tilde{h}_0 = 0. \quad (4.17)$$

Let

$$V_o = \begin{bmatrix} \tilde{h}_0 \\ \tilde{\phi}_0^- \end{bmatrix} \quad \text{and} \quad M = \begin{bmatrix} -C & 1 \\ G/K & -C \end{bmatrix}.$$

Then the previous set of equations (4.16)-(4.17) can be written as  $MV_o = 0$ . For a non-trivial solution we must have  $\det[M] = 0$ ; from this condition we obtain

$$C = \sqrt{G/K}, \quad (4.18)$$

and

$$\tilde{\phi}_0^- = C\tilde{h}_0. \quad (4.19)$$

From equation (4.2) we also obtain

$$-Ch_{0,x} + \Psi_{0,x}^+|_0 = 0,$$

or

$$-C\tilde{h}_0A_2 + (A_1\phi_a|_0 + B_{1-}\phi_b|_0) = 0. \quad (4.20)$$

To the next order we have

$$h_1 = \hat{A}_2(T)\tilde{h}_1e^{iKx} + \text{c.c.}$$

and

$$\begin{aligned} \Psi_{1,x}^-|_0 - Ch_{1,x} &= -h_{0,T}, \\ -C\Psi_{1,xY}^-|_0 + Gh_{1,x} &= -\Psi_{0,TY}^-|_0 + Gh_{0,x} - C\Psi_{0,xy}^+|_0 - U_{0,y}\Psi_{0,x}|_0, \end{aligned}$$

or

$$\begin{aligned} \tilde{\phi}_1 - C\tilde{h}_1 &= -\frac{1}{iK}A_{2,T}\tilde{h}_0, \\ -C\tilde{\phi}_1 + (g/k)\tilde{h}_1 &= -\frac{1}{iK}A_{2,T}\tilde{\phi}_0^- + A_2((G/K) - U_{,y}C(1/k))\tilde{h}_0 - \frac{1}{k}C(A_1\phi_{a,y} + B_{1-}\phi_{b,y}). \end{aligned}$$

Set  $V_1 = [\tilde{h}_1, \tilde{\phi}_1]^T$  and

$$W_1 = \begin{bmatrix} 0 \\ (G/K) - U_{,y}C/K \end{bmatrix}, \quad W_2 = \begin{bmatrix} 0 \\ -C/K\phi_{a,y} \end{bmatrix}, \quad W_3 = \begin{bmatrix} 0 \\ -C/K\phi_{b,y} \end{bmatrix};$$

then the previous set of equations can be written as

$$MV_1 = -\frac{1}{iK}A_{2,T}V_0 + A_2W_1 + A_1W_2 + B_{1-}W_3.$$

Let  $V^T = [C, 1]$ .  $V^T$  is chosen such that  $V^TM = 0$ . Then multiplying the previous equation with  $V^T$  yields

$$\frac{1}{iK}A_{2,T}\langle V^TV_o \rangle = A_2\langle V^TW_1 \rangle + A_1\langle V^TW_2 \rangle + B_{1-}\langle V^TW_3 \rangle, \quad (4.21)$$

where

$$\langle V^TV_o \rangle = C\tilde{h}_0 + \tilde{\phi}_0^- = 2C\tilde{h}_0 = 2C,$$

$$\langle V^TW_1 \rangle = (G/K) - U_{,y}C/K,$$

$$\langle V^T W_2 \rangle = -C/K \phi_{a,y},$$

$$\langle V^T W_3 \rangle = -C/K \phi_{b,y},$$

where with no loss of generality we have set  $\tilde{h}_o = 1$ ; here  $\phi_a, \phi_{a,y}, \dots$  refers to the values of these quantities at the interface.

Equation (4.21) is the amplitude equation. What is left to do is to recall the properties of  $A_2, A_1^\pm, B_1^\pm$  in order to cast the amplitude equation into a more convenient form. From the boundary condition at infinity, we will obtain a condition of the form  $B_{1+} = \mu A_{1+}$ , e.g., only one linear combination of the two Frobenius solutions will give a solution that dies at infinity. From equations (4.10) and (4.15) we have  $A_{1+} = A_{1-} = A_1, B_{1-} = B_{1+} - J$ , and from equation (4.20) we obtain  $-CA_2 + (A_1 \phi_a + B_{1-} \phi_b) = 0$ . Using these results, we can write

$$A_1 = \frac{C}{\phi_a + \mu \phi_b} A_2 + \frac{\phi_b}{\phi_a + \mu \phi_b} J, \quad (4.22)$$

$$B_{1-} = \frac{\mu C}{\phi_a + \mu \phi_b} A_2 - \frac{\phi_a}{\phi_a + \mu \phi_b} J. \quad (4.23)$$

We can therefore write the amplitude equation as

$$A_{2T} + \frac{i}{2} \left[ (U_{,y} - G/C) + C \frac{\phi_{a,y} + \mu \phi_{b,y}}{\phi_a + \mu \phi_b} \right] A_2 = i \left[ \frac{\phi_b \phi_{a,y} - \phi_a \phi_{b,y}}{\phi_a + \mu \phi_b} \right] J. \quad (4.24)$$

#### 4.2. Strong gravitation and arbitrary density ratio: $G \gg 1$ and $0 < r < 1$

We are now going to focus on cases for which  $G \gg 1$ , which are associated with small growth rate. As before, we use the time scaling  $\partial_t = \epsilon \partial_T - C \partial_x$ , where  $\epsilon$  is of the order of the linear growth rate (to be defined below). The governing equation is then equation (4.1), with the boundary condition now given by

$$\epsilon h_{,T} - C h_{,x} + \Psi_{,x}^+ = 0, \quad (4.25)$$

$$\epsilon h_{,T} - C h_{,x} + \Psi_{,x}^- = 0, \quad (4.26)$$

$$r \left[ \epsilon \Psi_{,Ty}^+ - C \Psi_{,xy}^+ - U_{,y}^+ \Psi_{,x}^+ \right] - \left[ \epsilon \Psi_{,Ty}^- - C \Psi_{,xy}^- \right] - G h_{,x} (1 - r) = 0. \quad (4.27)$$

We expand the surface elevation and stream function as:

$$\Psi = \epsilon^2 \Psi_0 + \epsilon^3 \Psi_1 + \dots \quad (4.28)$$

$$h = \epsilon^2 h_0 + \epsilon^3 h_1 + \dots \quad (4.29)$$

To zeroth order we then have again

$$(U - C) \nabla^2 \Psi_{0,x} - U_{,yy} \Psi_{0,x} = 0;$$

expanding in normal modes,  $\Psi_0 = A_2 \phi(y) e^{iKx} + \text{c.c.}$ , we have

$$\phi_{,yy} - \left[ K^2 - \frac{U_{,yy}}{U - C} \right] \phi = 0,$$

where we have again focused on the most unstable mode. Since we are dealing with the large  $G$  case, we know from equation (3.6) that the wave-numbers of the unstable modes must satisfy (in the limit of large  $G$ )

$$K \geq \frac{1-r}{1+r}G = \mathcal{A}_t G \gg 1 \quad (4.30)$$

(where  $\mathcal{A}_t$  is the Atwood number); we can then use the results from the WKBJ expansion discussed in Appendix A. These results show that the value of  $\Psi_0$  and  $\Psi_{0,y}$  at the interface is

$$\Psi_0|_0 = \left[ A_1(\sin(I_1)e^{-I_2} + \cos(I_1)e^{+I_2}) - \frac{1}{\pi}J \sin(I_1)e^{+I_2} \right] e^{iK(x-Ct)} + \text{c.c.} \quad (4.31)$$

$$\Psi_{0,y}|_0 = \left[ A_1(\sin(I_1)e^{-I_2} - \cos(I_1)e^{+I_2}) + \frac{1}{\pi}J \sin(I_1)e^{+I_2} \right] e^{iK(x-Ct)} + \text{c.c.}, \quad (4.32)$$

where  $I_1 \sim 1/K$  and  $I_2 \sim K \geq \mathcal{A}_t G \gg 1$  are defined in the Appendix. Unlike the linear case, we assumed that the phase change is  $J$ , defined as in equation (4.14) in the previous section (§4.1.2). We avoid repeating the inner scale calculations since they are identical to that for the small density ratio case. The slow time scale is now defined by the value of  $C_i$ , which is exponentially small and is given by expression (3.11). We will therefore define  $\epsilon \equiv e^{-2I_2}$ . Equations (4.31) and (4.32) can then be written as

$$\Psi_0|_0 = \left[ A_1 \cos(I_1) - \frac{1}{\pi}J \sin(I_1) + \epsilon A_1 \sin(I_1) \right] e^{iKx} + \text{c.c.}, \quad (4.33)$$

and

$$\Psi_{0,y}|_0 = -K \left[ A_1 \cos(I_1) - \frac{1}{\pi}J \sin(I_1) - \epsilon A_1 \sin(I_1) \right] e^{iKx} + \text{c.c.}, \quad (4.34)$$

where we have rescaled  $\Psi_0$  so that it is of order unity at the interface.

Writing the zeroth order stream function  $\Psi_0^-$  below the interface, and the surface elevation  $h_0$  as

$$\Psi_0^- = A_3 e^{iKx+Ky} + \text{c.c.}, \quad (4.35)$$

$$h_0 = A_2 e^{iKx} + \text{c.c.}, \quad (4.36)$$

the first order boundary conditions give us

$$M \cdot V_0 = 0, \quad (4.37)$$

where

$$M = \begin{bmatrix} -C & 1 & 0 \\ -C & 0 & 1 \\ -G(1-r) & rCK & CK \end{bmatrix}, \quad V_0 = \begin{bmatrix} A_2 \\ \Phi \\ A_3 \end{bmatrix}, \quad (4.38)$$

and  $\Phi = (2A_2 \cos(I_1) - \frac{1}{\pi}J \sin(I_1))$  is the amplitude of the stream function at the interface. Here we have discarded the  $U_y$  term since it is of order  $1/K$ . For a non-trivial solution, we must have  $\det(M) = 0$ . This leads us to the relations

$$C = \sqrt{G\mathcal{A}_t/K} \quad (4.39)$$

and

$$A_2 C = \Phi, \quad (4.40)$$

$$A_2 C = A_3. \quad (4.41)$$

At the next order, we have

$$(U - C)\nabla^2\Psi_{1,x} - U_{,yy}\Psi_{1,x} = \nabla^2\Psi_{0,T},$$

and by letting  $\Psi_1 = \hat{A}_1 e^{iKx} \phi_1(y)$ , we have

$$\hat{A}_1 \left[ \phi_{1,yy} - \left( K^2 + \frac{U_{,yy}}{U - C} \right) \phi_1 \right] = \hat{A}_{1,T} \frac{U_{,yy}}{U - C} \phi_0. \quad (4.42)$$

Since we are still in the large  $K$  limit, we can still use the WKBJ approximation for the above non-homogeneous equation. One needs to notice that the non-homogeneous term is going to be of order  $1/K^2$  everywhere except close to the critical layer, and that special care is needed to be taken there. Fortunately, the exact value of  $\phi_1$  at the interface is not needed — it is sufficient to know that the solution of equation (4.42) below and away from the critical layer is

$$\phi_1 = \hat{A}_{1a} \frac{1}{w} e^{+K \int_0^{yc} w dy'} e^{-Ky} + \hat{A}_{1b} \frac{1}{w} e^{-K \int_0^{yc} w dy'} e^{+Ky}, \quad (4.43)$$

where  $w = (K^2 - U_{,yy}/(U - C))^{1/2}$ , and where the values of  $\hat{A}_{1a}, \hat{A}_{1b}$  depend on  $A_{1T}$ , and can be obtained by matching with the inner solution at the critical layer. The second term in equation (4.43) is exponentially small (order  $\epsilon$ ), so that at the interface we have  $\phi_{1,y} = -K\phi_1$ ; this suffices for the remainder of our analysis. The stream function of the lower fluid  $\Psi_1^-$  and the elevation  $h_1$  at this order are

$$\Psi_1^- = \hat{A}_3 e^{iKx + Ky} + \text{c.c.},$$

$$h_1 = \hat{A}_2 e^{iKx} + \text{c.c.}$$

The boundary conditions at the interface are

$$M \cdot V_1 = -\frac{1}{iK} \partial_T W_1 + W_2, \quad (4.44)$$

(where  $M$  was defined in equation 4.38)

$$V_1 = \begin{bmatrix} \hat{A}_2 \\ \phi_1 \hat{A}_1 \\ \hat{A}_3 \end{bmatrix}, W_1 = \begin{bmatrix} A_2 \\ A_2 \\ -K(r\Phi + A_3) \end{bmatrix} = A_2 \begin{bmatrix} 1 \\ 1 \\ -(r+1)KC \end{bmatrix}, \quad (4.45)$$

and

$$W_2 = \begin{bmatrix} -\sin(I_1)A_1 \\ 0 \\ rKC \sin(I_1)A_1 \end{bmatrix}. \quad (4.46)$$

As before, let  $V^T = [-rCK, -CK, 1]$  where  $V^T$  is such that  $V^T M = 0$ . Multiplying equation (4.44) with  $V^T$ , we obtain

$$V^T W_1 = -2(1+r)CKA_2, \quad V^T W_2 = 2rCKA_2 \sin(I_1).$$

Hence, we arrive at the amplitude equation for large  $G$

$$\frac{1}{iK} V^T W_{1,T} = V^T W_2, \quad (4.47)$$

or

$$A_{2,T} = -iK \frac{r}{1+r} \sin(I_1) A_1, \quad (4.48)$$

with

$$CA_2 = 2A_1 \cos(I_1) - J \frac{1}{\pi} \sin(I_1). \quad (4.49)$$

The amplitude evolution can now be determined from equations (4.48)-(4.49).

## 5. Results

### 5.1. Preliminaries

For both cases we have considered, the amplitude equations to be solved in order to determine the nonlinear evolution of the unstable mode can be written in to the following more general form:

$$A_{2,T} + i\mathcal{C}_1 A_2 = i\mathcal{C}_2 J \quad (5.1)$$

$$A_2 = \mathcal{D}_1 A_1 + \mathcal{D}_2 J \quad (5.2)$$

$$J = \frac{K}{2\pi} \frac{U'_c}{U''_c} \int_{-\pi/K}^{+\pi/K} e^{-iKx} \int_{-\infty}^{+\infty} Z \, dY dx \equiv \langle e^{-iKx} Z \rangle \quad (5.3)$$

$$Z_{,T} + U'_c Y Z_{,x} - \tilde{\Psi}_{0,x} Z_{,Y} - \nu Z_{,YY} = U''_c \tilde{\Psi}_{0,x} \quad (5.4)$$

with

$$\lim_{Y \rightarrow \infty} Z = \left[ A_1 \frac{U''_c}{2U'_c} \frac{1}{Y} + \frac{U''_c}{2U'^2_c} \frac{1}{Y^2} A_{1,T} \right] e^{iKx} + c.c.$$

and

$$\tilde{\Psi}_0 = A_1 e^{iKx} + A_1^* e^{-iKx}$$

The equations above should be interpreted the following way. Equation (5.2) expresses the continuity of the normal velocity at the interface: It imposes the constraint that the phase and amplitude of the perturbation of the surface wave (given by  $A_2$ ) is the same as the perturbation of the wind (given by  $\mathcal{D}_1 A_1 + \mathcal{D}_2 J$ ) including the component that comes from the phase change at the interface. Equation (5.1) is Newton's law, or alternatively can be viewed as a statement about the continuity of pressure at the interface; it gives the growth of the amplitude  $A_2$  due to the out of phase component of the pressure. Equation (5.4) gives the evolution of the vorticity inside the critical layer that determines the phase change, and involves the non-linear term  $\tilde{\Psi}_{0,x} Z_{,Y}$ . The coefficients  $\mathcal{C}_1, \mathcal{C}_2, \mathcal{D}_1, \mathcal{D}_2, \in \Re$  are obtained from the linear theory, and are given in equations (4.22), (4.24), (4.48) and (4.49).  $\mathcal{C}_1$  and  $\mathcal{D}_2$  are terms that involve small correction to the real part of  $C$  due to the gradient of the velocity at the interface  $U_{,y}$  and due to the part of the pressure perturbation that is in phase with the traveling wave.  $\mathcal{C}_2$  and  $\mathcal{D}_1$  involve the part of the pressure perturbation that is out of phase with the traveling wave; their sign determines the nature of the instability.

Dropping the non-linear term in eq. (5.4) we obtain  $J = i\pi A_1$  in the linear case (Drazin & Reid 1981). Assuming an exponential growth rate  $A_i = e^{\gamma T} a_i$ , the above equation can be written as:

$$\pi \mathcal{C}_2 a_1 + (\gamma + i\mathcal{C}_1) a_2 = 0, \quad (5.5)$$

$$(\mathcal{D}_1 - i\pi \mathcal{D}_2) a_1 - a_2 = 0; \quad (5.6)$$

the growth rate then is given by

$$\gamma = -\frac{\pi\mathcal{C}_2\mathcal{D}_1}{\mathcal{D}_1^2 + \pi^2\mathcal{D}_2^2} - i\left(\frac{\pi^2\mathcal{D}_2\mathcal{C}_2}{\mathcal{D}_1^2 + \pi^2\mathcal{D}_2^2} + \mathcal{C}_1\right). \quad (5.7)$$

For a positive growth rate we therefore need to have  $\mathcal{C}_2\mathcal{D}_1 < 0$ .

We note as an aside that there are several conservation laws at work here.† First, the vorticity is conserved inside the critical layer  $\langle Z \rangle_{,T} = 0$ , which implies  $\langle Z \rangle = 0$  since the initial  $Z$  had infinitesimal amplitude. Second, by noting that  $\langle \Psi_{0,x} Z \rangle = iK(J^*A_1 - JA_1^*)$ , one can show that the following laws hold:

$$\frac{d}{dT} \{K|A_2|^2 - \mathcal{C}_2\mathcal{D}_1\langle YZ \rangle\} = 0; \quad (5.8)$$

$$\frac{d}{dT} \left\{KU_c''|A_2|^2 + \frac{1}{2}\mathcal{C}_2\mathcal{D}_1\langle Z^2 \rangle\right\} = -\mathcal{C}_2\mathcal{D}_1\nu\langle Z_{,Y}^2 \rangle; \quad (5.9)$$

$$\frac{d}{dT} \left\{\mathcal{D}_1\mathcal{C}_2\langle(\tilde{\Psi}_0 + \frac{1}{2}U_c'Y^2)Z\rangle + \mathcal{D}_2\mathcal{C}_2|J|^2 - \mathcal{C}_1|A_2|^2\right\} = \nu U'\mathcal{C}_2\langle Z \rangle. \quad (5.10)$$

Recalling that the velocity inside the critical layer is given by  $[u - C, w] = [\epsilon U_c'Y + \epsilon^2(1/2U_c''Y^2 + \Psi_{2,Y}) + \dots, \epsilon^2\Psi_{0,x} + \dots]$  we can identify the first relation (eq. 5.8) to correspond to the conservation of momentum. Combining equations (5.8) and (5.9), we obtain the conservation of enstrophy inside the critical layer,

$$\frac{d}{dT} \langle (U_c''Y + Z)^2 \rangle = -\nu\langle Z_{,Y}^2 \rangle. \quad (5.11)$$

The third equation (5.10) can be regarded as a statement of the conservation of energy.

## 5.2. Quasi-steady state

An interesting limit in the set of our equations is when the rescaled viscosity is large enough to play a dominant role inside the critical layer. With this assumption we can drop the time derivative term in equation (4.13); the functional form of  $Z$  then just depends on the value of  $A_1$ , which then makes  $J$  just a function of  $A_1$ . More specifically we have

$$\nu Z_{,YY} + \tilde{\Psi}_{0,x}Z_{,Y} - U_c'YZ_{,x} = -U_c''\tilde{\Psi}_{0,x}; \quad (5.12)$$

by letting  $A_1 = R(T)e^{i\Theta(T)}$  and  $\xi = Kx + \Theta$ , we have

$$\nu Z_{,YY} - 2RK \sin(\xi)Z_{,Y} - U_c'KYZ_{,\xi} = 2U_c''RK \sin(\xi). \quad (5.13)$$

Let  $Y = \sqrt{2\eta}(R/U_c')^{1/2}$ ,  $Z = \sqrt{R/2U_c'U_c''}\hat{Z}(\xi, \eta)$  and  $\lambda = \nu\sqrt{U_c'}/(K(2R)^{3/2})$ ; we then obtain

$$\lambda\hat{Z}_{,\eta\eta} - \sin(\xi)\hat{Z}_{,\eta} - \eta\hat{Z}_{,\xi} = 2\sin(\xi); \quad (5.14)$$

Equation (4.14) then becomes

$$J = \frac{K}{2\pi} \frac{U_c'}{U_c''} \int_{-\infty}^{+\infty} \int_{-\pi/K}^{+\pi/K} e^{-iKx} Z dx dY = \frac{1}{2\pi} R \cdot e^{i\Theta} \int_{-\infty}^{+\infty} \int_{-\pi+\Theta}^{+\pi+\Theta} e^{-i\xi} \hat{Z} d\xi d\eta$$

† In the equations (5.8), (5.9), and (5.10), the integration over  $x$  was assumed to be taken first.

$$\begin{aligned}
 &= \frac{1}{2\pi} R \cdot e^{i\Theta} \left[ \int_{-\infty}^{+\infty} \int_{-\pi}^{+\pi} \cos \xi \hat{Z} d\xi d\eta - i \int_{-\infty}^{+\infty} \int_{-\pi}^{+\pi} \sin \xi \hat{Z} d\xi d\eta \right] \\
 &= -i \frac{1}{2\pi} A_1 \int_{-\infty}^{+\infty} \int_{-\pi}^{+\pi} \sin \xi \hat{Z} d\xi d\eta
 \end{aligned}$$

or

$$J = -i A_1 \Phi_1(\lambda)$$

with

$$\Phi_1(\lambda) = \frac{1}{2\pi} \int_{-\pi}^{+\pi} \int_{-\infty}^{+\infty} \sin \xi \hat{Z} d\eta d\xi.$$

$\Phi_1(\lambda)$  was first studied numerically by Haberman (1972). Its values range from  $-\pi$  for  $\lambda \rightarrow \infty$  to 0 for  $\lambda \rightarrow 0$ . Its asymptotics for  $\lambda \rightarrow 0$  and  $\lambda \rightarrow \infty$  are given by

$$\Phi(\lambda) = \begin{cases} -a_1 \lambda + a_2 \lambda^{3/2} + O(\lambda^2) & \lambda \ll 1 \\ -\pi + b_1 \lambda^{-4/3} + O(\lambda^{-8/3}) & \lambda \gg 1 \end{cases} \quad (5.15)$$

where  $a_1 = 5.5151\dots$ ,  $a_2 = 4.2876\dots$  and  $b_1 = 1.6057\dots$ . The derivation for the above asymptotics can be found in (Churilov & Shukman 1996). We illustrate the behavior of  $\Phi(\lambda)$  in figure. (1), constructed by combining numerical evaluation with the aforementioned asymptotics.

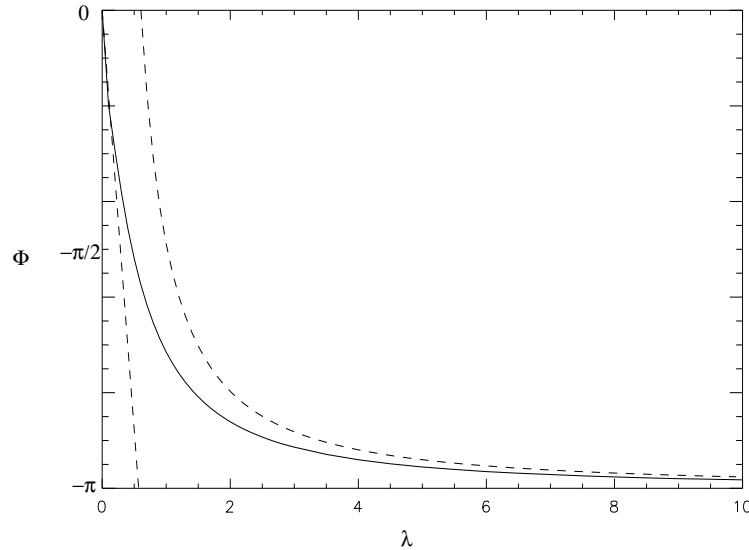


FIGURE 1. The Haberman function

The amplitude equation then can be written as

$$A_{2,T} + iC_1 A_2 = C_2 A_1 \Phi \left( \frac{\nu \sqrt{U'_c}}{K(2|A_1|)^{3/2}} \right)$$

, with

$$A_2 = \mathcal{D}_1 A_1 + i\mathcal{D}_2 A_1 \Phi \left( \frac{\nu \sqrt{U_c'}}{K(2|A_1|)^{3/2}} \right).$$

We have thus ended up with an ordinary differential equation for the amplitude of the wave. By setting  $A_1 = R(T)\exp[i\Theta(T) - i\mathcal{C}_1 T]$ , and after some algebra, one can show that

$$\left( \mathcal{D}_1^2 + \mathcal{D}_2^2 \Phi \tilde{\Phi} \right) R_{,T} = \mathcal{D}_1 \mathcal{C}_2 R^2 \Phi, \quad (5.16)$$

$$\left( \mathcal{D}_1^2 + \mathcal{D}_2^2 \Phi \tilde{\Phi} \right) \Theta_{,T} = \mathcal{C}_2 \mathcal{D}_2 \Phi \tilde{\Phi}, \quad (5.17)$$

where  $\tilde{\Phi} = (R\Phi)_{,R}$ . For large  $R$  at late times we can conclude that

$$|A_2| \sim |A_1| \equiv R \sim \nu T^{2/3} \quad (5.18)$$

and

$$\Theta \sim \nu^2 T^{-1}. \quad (5.19)$$

This is one of the basic results of our calculations. As we are going to show later, this result becomes valid for later times even for cases for which the rescaled viscosity is smaller than one. An important implication of this result is that the amplitude grows with an algebraic power instead of the initial exponential variation. Another important feature is that the growth rate linearly depends on the viscosity, unlike the case in linear theory. (In linear theory, a weak viscosity was giving the same phase change “ $-i\pi$ ”, but the resulting growth rate was independent of  $\nu$ .) Finally we note that the phase of the waves  $\Theta$ , goes asymptotically to zero at late times according to equation (5.19).

### 5.3. Numerical Results

Next we investigate the weakly non-linear evolution of the wave by solving the set of equations (5.1-5.4) numerically. To solve the advection equation (5.4), we used a code which is spectral in  $x$  and finite difference in  $Y$ . The domain we used was  $(-50, 50)$  in  $Y$  and  $(0, 2\pi)$  in  $x$ . Up to 1024 grid points were used in the  $Y$  direction and 63 modes were kept in  $x$ . The boundary conditions were satisfied to order  $1/Y$ , although the asymptotic behavior of  $Z$  was taken into account when we evaluated the integral in equation (5.3). The code was tested by comparing with a fully pseudo-spectral code as well as with already published results.

Before we begin solving the amplitude equations, however, we re-scale our system so that we are left with a minimum number of free parameters. As in the previous section, by letting  $Z = U''/\sqrt{U'}\tilde{Z}$ ,  $Y = \eta/\sqrt{U'}$ ,  $T = \tau/(\sqrt{U'}k)$ ,  $\xi = Kx$  and  $\nu = \nu'/\sqrt{U'}$  we obtain the following equation to be solved:

$$\tilde{Z}_{,\tau} + \eta \tilde{Z}_{,\xi} - \tilde{\Psi}_{0,\xi} \tilde{Z}_{,\eta} - \nu' \tilde{Z}_{,\eta\eta} = \tilde{\Psi}_{0,\xi},$$

with

$$J = \frac{1}{2\pi} \int_{-\pi}^{+\pi} \int_{-\infty}^{+\infty} e^{-i\xi} \tilde{Z} d\eta d\xi.$$

Furthermore, by rescaling  $A_1$  to  $|\mathcal{D}_1|^2/|\mathcal{C}_2|^2 A_1$ , and  $A_2$  to  $|\mathcal{D}_1|/|\mathcal{C}_2|^2 A_2$ , we can always scale our system so that  $\mathcal{D}_1 = 1$  and  $\mathcal{C}_2 = -1$ . Finally, the coefficient  $\mathcal{C}_1$  can always be set to zero by performing a Galilean transformation ( $\tau \rightarrow \tau + \mathcal{C}_1 \xi$ ) and shifting the critical

layer by  $Y \rightarrow Y - C_1$ . The last transformation corrects the position of the critical layer to order  $\epsilon$ , and justifies the neglect of the corresponding terms in §4.2. We are left therefore with one independent parameter,  $\mathcal{D}_2$ , to investigate; this parameter is a measure of the feedback of the gravity wave to the critical layer ( $\mathcal{D}_2 = 0$  gives the “free” evolution of a critical layer uncoupled from gravity waves). In the following, we examine five cases, for five values of  $\mathcal{D}_2$ .

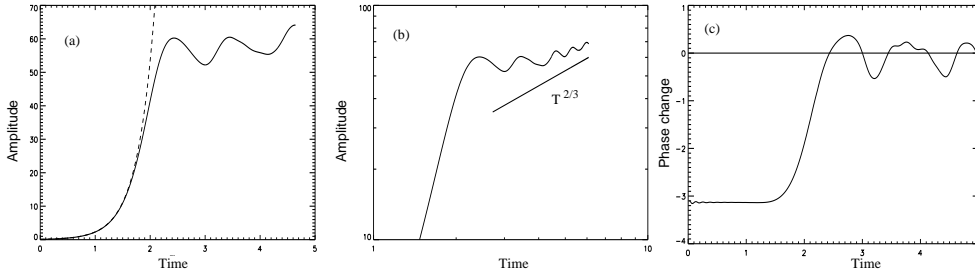


FIGURE 2. The evolution of the wave amplitude  $|A_1|$  (panels [a] and [b]), and of the phase change across the critical layer (panel [c]), as a function of time. The dashed line panel [a] gives the linear prediction; the solid line in panel [b] is intended to illustrate  $T^{2/3}$  scaling.

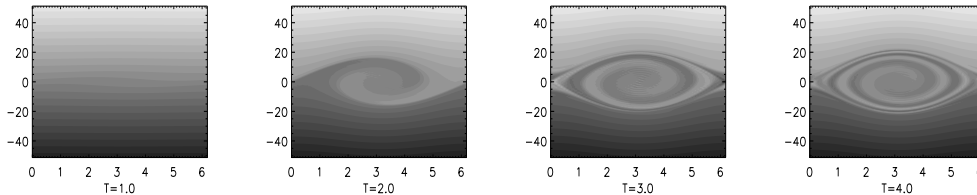


FIGURE 3. Time sequence of the evolution of the vorticity inside the critical layer for  $\mathcal{D}_2 = 0$ , using a grey-scale representation for the vorticity.

We first examine  $\mathcal{D}_2 = 0$  case, e.g. the evolution of a ‘free critical layer’. In figure (2a) we plot the amplitude as a function of time; the dashed line gives the linear prediction. The amplitude grows exponentially for early times, but as non-linearities become important the growth rate decreases, and an oscillatory behavior begins. figure (2b) shows the same thing, but plotted on a log-log scale, and compared with the  $T^{2/3}$  scaling; we note that the agreement is good for later times, although the persistence of the oscillations indicate that viscosity is not yet fully dominant. Figure (2c) gives us more information about the system; here we plot the phase change  $\Im\{-J/A_1\}$  as a function of time. The phase change (which is responsible for the instability) remains constant, and equal to  $-\pi$ , in the linear regime; in the non-linear regime it drops to zero and then oscillates around this value. In figure (3) we display the evolution of the total vorticity  $\tilde{Z} + \eta$  inside the critical layer, using a grey-scale representation; time frame were taken every 0.5 time units (the first panel is at  $T = 1$ ). The vorticity of the mode rises, as predicted by the linear theory, by extracting vorticity from the mean flow. (From eqs. (5.9) and (5.11) we know that the total vorticity and enstrophy are conserved; therefore the increase of  $Z^2$  must lead to a decrease of  $ZY$ .) As the non-linear term becomes important, the mean flow advects the vorticity in the vertical direction, leading to the ‘winding up’ motion seen in the panels with  $T \geq 2$ , forming the cat’s eyes pattern. The imaginary part of the integral  $J$  (eq. (5.3)) expresses the excess of vorticity of the right side of each panel,

from the left. After the first turnover, the vorticity is redistributed inside the critical layer more evenly, leading to smaller values of  $J$ . Comparing figure (2) with figure (3), it can be seen that deviations from linearity and the  $-i\pi$  phase change start when the vertical motion begins, and the phase change has dropped to zero when the first full turn over has been completed. At later times and after a few turnovers, small scale structure has been generated in the form of a ‘twisted’ vortex sheet with sharp boundaries. As this procedure carries on, at some point in time, viscosity (now matter how small) will become important, and the advection terms in eq. (5.4) will be balanced by the diffusion of vorticity; at that point, the asymptotic behavior predicted by the quasi-steady state for large times can be shown to hold.

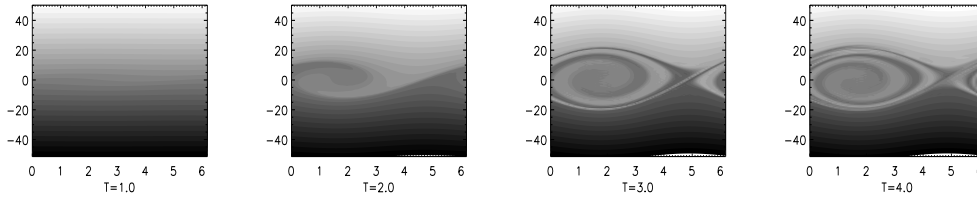


FIGURE 4. As in figure (3), but for  $\mathcal{D}_2 = 0.1$

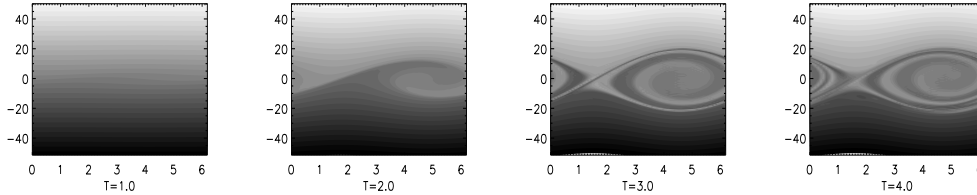


FIGURE 5. As in figure (3), but for  $\mathcal{D}_2 = -0.1$

Next we investigate the effect of non-zero  $\mathcal{D}_2$ . The cases we will examine will be for  $\mathcal{D}_2 = \pm 0.1$  and  $\pm 0.3$ . We start with the two cases  $\mathcal{D}_2 = \pm 0.1$ ; here we note that for  $\mathcal{D}_2 = -0.1$ , linear theory predicts a right traveling wave, but for  $\mathcal{D}_2 = 0.1$  predicts a left traveling wave. In figures (4) and (5) we show grey-scale representations of the evolution of vorticity for these two cases. We see that the result is two traveling vortices, as predicted by the linear theory, but the phase velocity is decreasing with time and the vortices seem to stop at a distance  $\pm\pi/2$  from their initial position. This is in agreement with the quasi-steady limit, which predicts that the phase  $\Theta(T)$  in equation (5.19) should decrease as  $T^{-1}$ . Small scale differences appear in the vorticity field when compared to figure (3), but these seem to be minor.

By considering lightly larger values of  $\mathcal{D}_2$  ( $= \pm 0.3$ ), we can obtain an indication of how this affects the amplitude of the wave. In figures. (6)-(7) we plot again grey-scale representations of the vorticity for four different times for the  $\mathcal{D}_2 = 0.3$  and  $\mathcal{D}_2 = -0.3$  cases, respectively. The linear growth rate is 1.8 times smaller, so the plots are at later times than the previous cases shown. Differences in the evolution of the vorticity can be seen especially at the ‘saddle point’ (the point where the two vortices meet).

A more quantitative appreciation of the time evolution of the wave amplitude can be obtained by directly plotting the evolution of the amplitudes  $A_1$  and  $A_2$  for the four

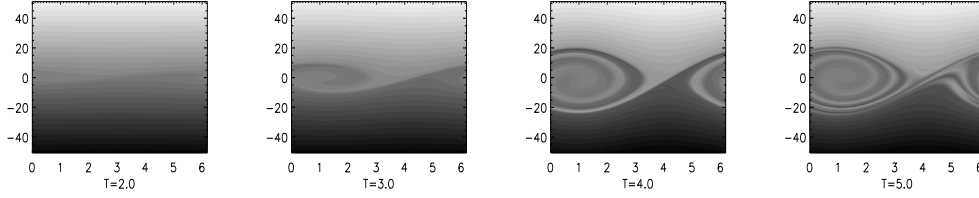


FIGURE 6. As in figure (3), but for  $\mathcal{D}_2 = 0.3$

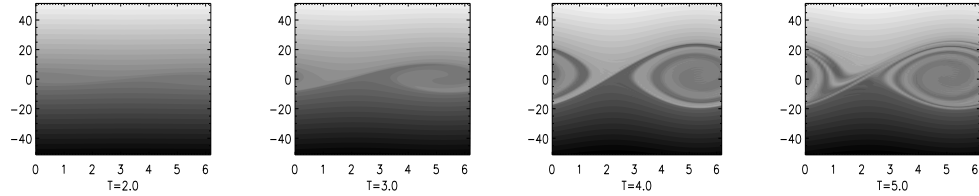


FIGURE 7. As in figure (3), but for  $\mathcal{D}_2 = -0.3$

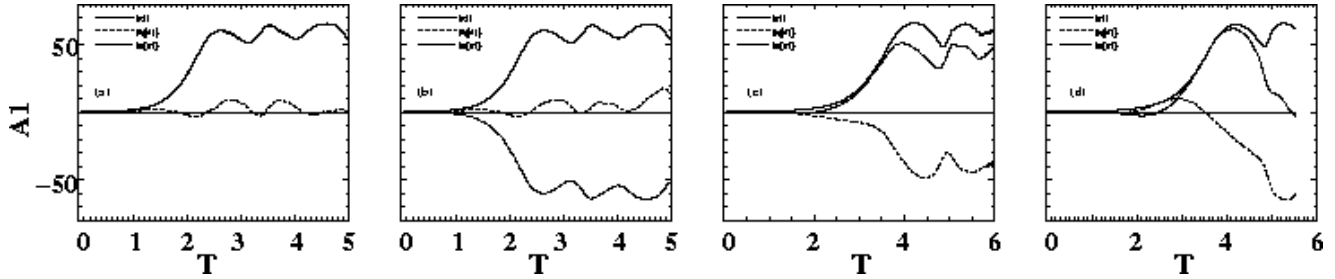


FIGURE 8. Evolution of the wave amplitude  $|A_1|$  for the four cases,  $\mathcal{D}_2 = 0.1$  (panel [a]),  $-0.1$  (panel [b]),  $0.3$  (panel [c]), and  $-0.3$  (panel [d]). In each panel, the solid lines show the magnitude of the amplitude, while the two sets of dashed lines show the evolution of the real and imaginary parts of the amplitude.

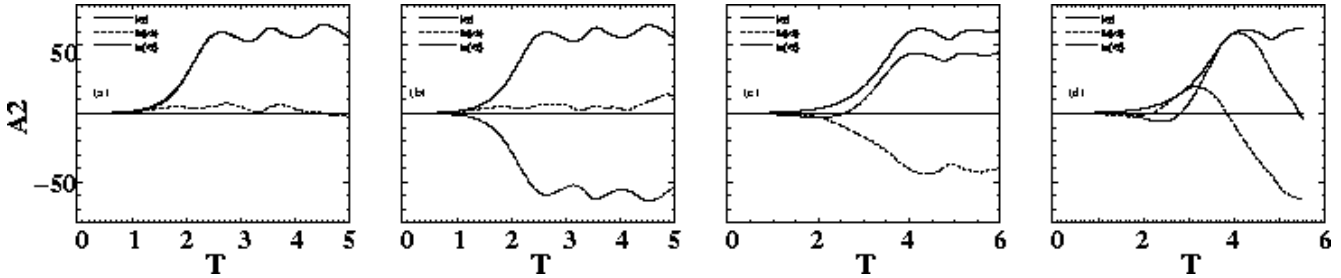


FIGURE 9. As in figure (8), but for wave amplitude  $|A_2|$ .

cases of non-zero  $\mathcal{D}_2$  we have examined, as shown in figures (8) and (9). In all panels, we show both the (unsigned) wave amplitude magnitude, as well as the real and imaginary parts of the amplitude; each panel of each figure corresponds to a different value of  $\mathcal{D}_2$ , as indicated.

Consider first the cases  $\mathcal{D}_2 = \pm 0.1$ . The fact that a positive imaginary part is dominant in panels [a] of figures (8)-(9), and a negative imaginary part in panels [b] of figures (2)-

(8), just expresses the fact that in this case, the two vortices moved by a quarter of the wave length and then stopped. We note that the magnitude of the amplitude at the point where the oscillations start (e.g., the peak of the ‘first bump’) does not seem to have been affected by the value of  $\mathcal{D}_2$ . Now consider  $\mathcal{D}_2 = \pm 0.3$ . We mentioned just above the appearance of small-scale differences in the grey-scale representations of the vorticity field as the magnitude of  $\mathcal{D}_2$  is increased; however, the quantitative plots of the wave amplitude show that these differences in the small-scale structures do not seem to affect the evolution of the amplitudes  $A_1$  and  $A_2$ : for example, in panels [c] of figure (8), we see that the value of  $A_1$  at which the first bounce of the amplitude occurs does not seem to depend strongly on the value of  $\mathcal{D}_2$ . We conclude therefore that the basic features of the weakly non-linear evolution of the unstable mode are not affected by the exact value of  $\mathcal{D}_2$ , at least in the examined range  $-0.3 \leq \mathcal{D}_2 \leq 0.3$ .

## 6. Mixing in the cat’s eye

In the previous sections we have examined the cat’s eye vortices in the nonlinear evolution of the critical layer in the wind coupled to a surface wave. We have found that the general flow structure to be similar to those in cases without coupling to the gravity waves. Such vortical structures are typical of the weakly nonlinear evolutions of parallel flows (Balmforth & Piccolo 2001). However, their mixing properties may be very different (depending on the details of the underlying flow) in spite of great similarity in the general flow features. We thus investigate the mixing due to these cat’s eyes from the weakly nonlinear amplitude equations for a few different cases.

In our amplitude equation 5.4, the vorticity  $Z$  is advected by velocity  $(u, v) = (Y, -\Psi_{0x})$ , with  $\Psi_0 \equiv A_1 e^{iKx} + \text{c.c.}$ . Thus the particle trajectories  $(x(x_0; t), y(y_0; t))$  satisfy equations

$$\frac{dx}{dt} = u = Y, \quad (6.1)$$

$$\frac{dy}{dt} = v = a_0(t) \sin(kx + \phi(t)), \quad (6.2)$$

where  $\mathbf{x}_0 \equiv (x_0, y_0)$  is the initial particle position and  $a_0(t)$  and  $\phi(t)$  are such that  $ikA_1 \equiv a_0(t)e^{i\phi(t)}$ .

If  $A_1$  is constant in time, equations (6.1)-(6.2) reduce to the equations of motion for a pendulum, only in this case the particle trajectory is not restricted to a cylindrical surface, and can move from eddy to eddy. We can calculate the strain rate of such a flow by first linearizing equations (6.1)-(6.2) for an infinitesimal separation between two particles  $\delta\mathbf{x}$ ,

$$\frac{d\delta\mathbf{x}}{dt} = (\delta\mathbf{x} \cdot \nabla)\mathbf{v} = \begin{pmatrix} 0 & 1 \\ ka_0 \cos(kx(\mathbf{x}_0; t) + \phi) & 0 \end{pmatrix} \delta\mathbf{x} \quad . \quad (6.3)$$

$\lambda_0$ , which is the negative determinant of the matrix in equation (6.3), is interpreted as the combination of strain and rotation:  $\lambda_0(\mathbf{x}_0) = ka_0 \cos(kx(\mathbf{x}_0; t) + \phi)$ . After time-averaging over the tracer trajectories,  $\langle \lambda_0 \rangle$  is only a function of the initial position of the tracer, and positive  $\langle \lambda_0 \rangle$  implies the possibility for a positive Lyapunov exponent for that initial position; negative  $\langle \lambda_0 \rangle$  implies that rotation is dominant over strain. We have calculated the time-averaged  $\langle \lambda_0 \rangle$  for each initial position  $\mathbf{x}_0$  in the vorticity for a simple case in Balmforth & Piccolo (2001) (figure 10(a)). The corresponding plot for the case of coupling the shear flow to the gravity surface waves is shown in figure 10(b).

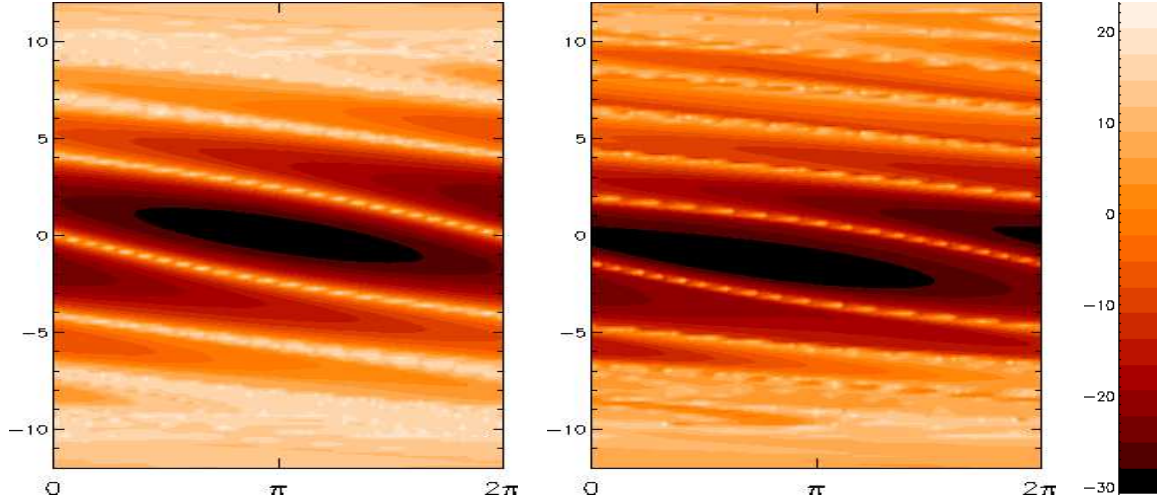


FIGURE 10. (a):  $\langle \lambda_0 \rangle$  for the critical layer without coupling to the gravity wave ( $\mathcal{D}_2 = 0$  in (Balmforth & Piccolo 2001)). (b):  $\langle \lambda_0 \rangle$  for the critical layer coupled to the gravity wave ( $\mathcal{D}_2 = 0.2$ ).

The relation between  $\langle \lambda_0 \rangle$  and the finite time Lyapunov exponent may not be straightforward, and can depend sensitively on the prescribed flow. In general, some correction to  $\langle \lambda_0 \rangle$  can be made so that it is closer to the Lagrangian description (Boffetta, Lacorata, Redaelli & Vulpiani 2001).

$$\lambda = \langle \lambda_0 \rangle + \langle \lambda_1 \rangle, \quad (6.4)$$

$$\lambda_1 = \sqrt{\frac{d\psi_{xy}^2}{dt} - \frac{d\psi_{xx}}{dt} \frac{d\psi_{yy}}{dt}}, \quad (6.5)$$

where  $\psi$  is the stream function of the flow. In our case  $\lambda_1 = 0$ , and thus we expect  $\langle \lambda_0 \rangle$  to be a good indicator of the finite time Lyapunov exponent, which we have also calculated and shown in figure (11) for the two cases in figures (10)a,b.

From figures (10)-(11) we conclude that the coupling of shear flow to the surface wave induces nonlinear evolution in such a fashion that more chaotic mixing may occur in the latter case; this conclusion follows from the observation that there appear to be more stripes of positive Lyapunov exponent in the driven surface wave case.

In situations where the passive tracers are weakly diffusive, the asymptotic mixing property is determined by the combination of slow diffusion and fast advection. If we define  $\theta$  as the tracer concentration, we can write down the equation for the weakly diffusive tracer in the above flow field, (equations 6.1 and 6.2),

$$\frac{\partial \theta}{\partial t} + y \partial_x \theta + (a_0(t) \sin(kx + \phi(t)) \partial_y \theta = \frac{1}{\text{Pe}} \nabla^2 \theta, \quad (6.6)$$

where  $\text{Pe} \equiv U_0 l / \kappa$  is the Peclet number, with  $U_0$  and  $l$  the characteristic velocity and length defined in previous section, and  $\kappa$  the molecular diffusivity of the tracer. The particle dispersion (variance), often indicative of mixing property of parallel flow, is defined as

$$\sigma^2 \equiv \langle x^2 \rangle - \langle x \rangle^2, \quad (6.7)$$

where  $\langle x \rangle$  and  $\langle x^2 \rangle$  are, respectively, the first and second longitudinal moments of the

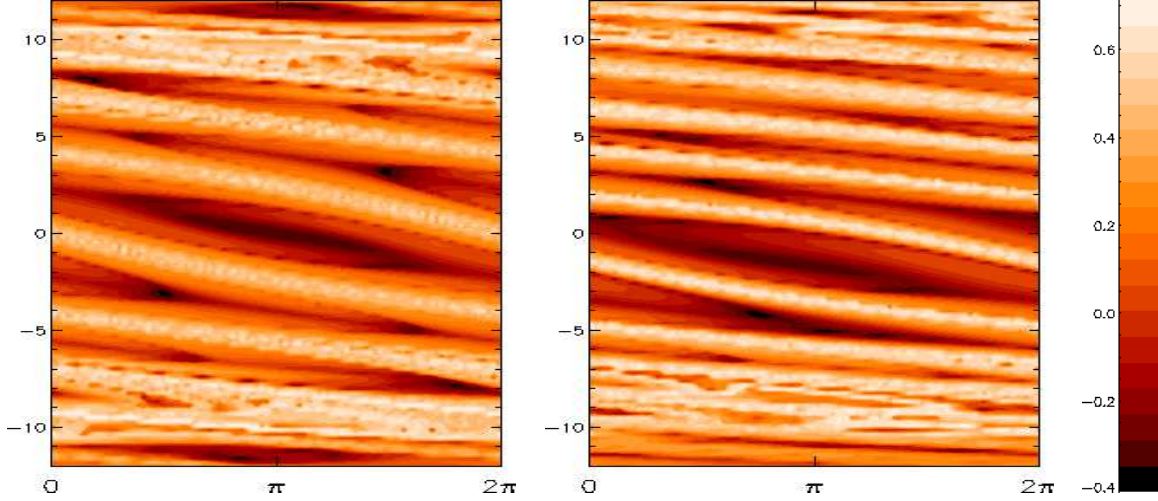


FIGURE 11. (a): Finite time Lyapunov exponent the un-coupled case  $\mathcal{D}_2$  in Balmforth & Piccolo (2001). (b): Finite time Lyapunov exponent for our case  $\mathcal{D}_2 = 0.2$ .

concentration field  $\theta$

$$\langle x \rangle \equiv \int x \theta d^2x, \quad \langle x^2 \rangle \equiv \int x^2 \theta d^2x.$$

If the flow is weak and diffusion is strongly dominant over advection, particles undergo random walks and their dispersion ( $\sigma$ ) increases linearly with the square root of time:  $\sigma = (2t/\text{Pe})^{1/2}$ . On the other hand, if the shear flow is strong and irregular in time, the particles will be in a super-diffusive regime during which the dispersion grows faster than that for ballistic transport ( $\sigma \sim t$ ). In cases where the flow is bounded and time-independent, the super-diffusive regime eventually gives way to yet another diffusive (Taylor) regime with a larger effective diffusivity than molecular diffusion.

For a time-dependent velocity field, the super-diffusive regime will be the asymptotic limit of particle transport, and chaotic mixing may be found instead. To examine how the time dependence of the flow affects the particle mixing in our case, we have integrated equation (6.6) using a particle method ((Latini & Bernoff 2001) and references therein) with  $a_0(t)$  and  $\phi(t)$  resembling those from solving the amplitude equations. We place  $10^5$  particles at an initial position close to the separatrix around the core, solve for their positions according to equation (6.6) for  $\text{Pe} = 10^5$ , and record their positions from which we can calculate the particle dispersion. In our case (equations 6.1 and 6.2), ballistic transport is expected (and confirmed numerically) if there is no time variation in  $A_1$ .

Figures (12) show the dispersion  $\sigma$  versus time for three time dependences of the amplitude  $a_0$ . The solid line is for an exponential growing amplitude which saturates to  $a_0 \sim 1$  at  $t \sim 100$ , and then oscillates periodically with a fluctuation amplitude of 0.2 and a period of 6. The long dashed line is the same except the oscillatory period is 65. The dash-dotted line is the same as the first two cases except the oscillation is replaced by an algebraic growth proportional to  $t^{2/3}$ . We clearly see that the early time dependence from simulations is verified as the diffusive regime, where  $\sigma = (2t/\text{Pe})^{1/2}$ . We also observe that the long time asymptotics for all three cases are at least super-diffusive, with  $\sigma \sim t^{3/2}$  for cases 1 and 2, while for case 3, where the amplitude grows as  $t^{2/3}$ , the dispersion is close to  $\sigma \sim t^2$ .

These results are consistent with anomalous diffusion found in other two-dimensional

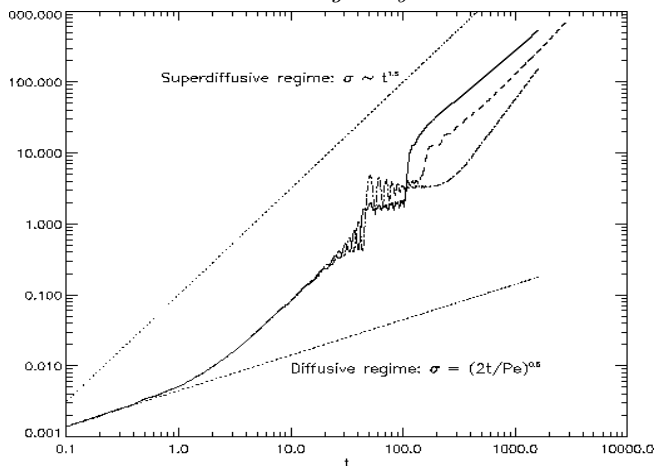


FIGURE 12. Particle dispersion for three time-varying amplitudes.

flows (Venkataramani, Antonsen & Ott 1998). The temporal periodicity in the flow creates the possibility for KAM regions to coexist with chaotic regions, and thus the anomalous particle transport. However, for the third case, the time variation of the flow is not periodic, and there does not exist any KAM regions, and thus the particle transport is more super-diffusive.

## 7. Discussion and Conclusion

In this paper, we have extended our earlier linear analysis of the resonant interaction between a wind and interface waves to the weakly nonlinear regime.

Our principal result is the demonstration that the exponential growth of unstable resonant waves characteristic of the linear regime transitions to algebraic growth in the weakly nonlinear regime, with the wave amplitude growing as  $t^{2/3}$ , similar to the cases without coupling with the gravity waves. We also find that the algebraic growth is linearly proportional to the weak viscosity inside the critical layer.

Before continuing, we return to examine our assumptions which allowed us to carry out the weakly nonlinear analysis. As noted earlier, our analysis is carried out around the point where the most unstable mode becomes marginally stable (which corresponds to, for example, the condition  $\mathcal{T}G = 1/4$  for  $r = 0$ ). In terms of dimensional parameters, this means that we conduct our analysis for values of the maximum wind velocity  $U$  in the range

$$U_1 < U < U_2, \quad (7.1)$$

where  $U_1$  is found from the criterion that all the perturbations are neutral in the presence of surface tension for  $r = 0$ :

$$\mathcal{T}G = \frac{\sigma}{\rho_2 U_1^2 l} \frac{gl}{U_1^2} = \frac{1}{4}, \quad (7.2)$$

and  $U_2$  is defined as the upper bound on the maximum wind speed for which only one of the unstable modes has crossed the stability boundary. This latter condition arises from the assumption of a periodic domain, which leads to a discrete spectrum, and is crucial in numerical simulations.

First we note that equation 7.2 gives a lower bound on maximum wind velocity ( $U_2$ ) that is independent of the length scale ( $l$ ) of the wind profile. Equation (7.2) thus gives

a general lower bound on the maximum wind velocity  $U$  for which our analysis applies. For the air-on-water case, we substitute  $\rho_2 = 1 \text{ gm cm}^{-3}$ ,  $g = 980 \text{ cm s}^{-2}$ , and  $\sigma = 72.8 \text{ dynes cm}^{-1}$  into the above equation, and obtain a lower bound for the wind velocity:  $U_1 \sim 0.2 \text{ m s}^{-1}$ . For  $U$  below this value in air-on-water system, system is stable (Alexakis, Young & Rosner 2002). The upper bound on the maximum wind velocity so that our analysis applies can be explicitly expressed in terms of size of the periodic domain  $l_b$ ,  $\sigma$ ,  $g$  and  $\rho_2$

$$U_2(l_b) \sim \max \left( \sqrt{\frac{4\pi^2\sigma + g\rho_2 l_b^2}{2\pi\rho_2 l_b}}, \sqrt{\frac{16\pi^2\sigma + g\rho_2 l_b^2}{4\pi\rho_2 l_b}} \right), \quad (7.3)$$

where  $l_b$  is of the same order as the wind characteristic length:  $l_b \sim \mathcal{O}(l)$ . For the air-water case, we find that the upper bound  $U_2$  to be a few times larger than  $U_1$ , and thus we expect that our results will be a good approximation for winds with velocity up to  $U_2 \sim 1 \text{ m s}^{-1}$ . Winds of this magnitude cause ripples on water-surfaces but not any wave breaking.

Within the range of validity of our analysis, we can further examine when the evolution transitions from linear to nonlinear regimes, e.g., the transition from exponential to algebraic growth. For small density ratio (the air-over-water case), and for high Reynolds numbers (for which the results from §5.3 hold), this transition happens when the amplitude is  $A_2 \simeq 60$ . Re-constructing the dimensional amplitude, we conclude that the perturbation grows exponentially until its amplitude reaches  $h/l \sim 60\epsilon^2 \simeq 6 \cdot 10^{-5}$ , where  $l$  is the length scale of the wind (see §2;  $l$  is of the same order as the most unstable wavelength) and  $\epsilon = r = 10^{-3}$  is the air-over-water density ratio. If, on the other hand, the rescaled Reynolds number is small enough so that the quasi-steady state approximation (§5.2) is appropriate, then the transition will happen when the Haberman parameter  $\lambda$  is close to one ( $\lambda \simeq 1$ ; see figure 1). This implies that the transition amplitude scales as  $h/l \sim 1/Re$ , which is still very small since we are in the almost inviscid limit. The key point, however, is that in both cases, the amplitude at which the transition in behavior occurs is extremely small, and most likely is too small to be observed in numerical simulations. Thus, any linear growth observed in simulations can only result from wind with maximum velocity much greater than  $0.2 \text{ m s}^{-1}$ . Our results also indicate that the energetic estimate provided by Miles (1999) should only work only when the wind is much stronger than  $0.2 \text{ m s}^{-1}$ .

Furthermore, we note that the linear regime (e.g., exponential growth) would be observable if the wind velocity is larger than order one. For example, if  $1 \gg G^{-1} \gg r$ , then the linear growth rate will be larger than order  $r$ ; this implies a different scaling than  $\epsilon = r$ . (The derivation of the new scaling is straightforward, but depends on the how the free parameter  $G$  scales with  $\epsilon$  (e.g.,  $G \sim \epsilon^\alpha$ ); since this is essentially unknown, we have chosen not to pursue this calculation further.) In cases for large  $U$ , we would then expect both the exponential and the algebraic growth rates to be observable in carefully conducted laboratory or numerical experiments.

For astrophysical cases, for which the density ratio is not so small ( $r \simeq 0.1 \sim 0.5$ ), it is much easier to capture both scalings (exponential and algebraic), in either numerical and experimental work. That is, following the previous arguments, the transition amplitude between the two scaling regimes is  $h/l \sim \mathcal{O}(0.1)$ , and can be easily varied by changing the magnitude of the wind. Numerical simulations are therefore obtainable to follow the fully non-linear development of the waves; and this is what we intend to do in our future work. Furthermore, it remains an open question as to whether the above discussion

applies to situations in which the physical domain is not periodic, such as in laboratory experiments.

Finally, we note that we have obtained an interesting result, namely the enhanced mixing at the ‘saddle points’ separating successive cat’s eyes within the unstable interface; this enhanced mixing (which we studied by means of inserting Lagrangian tracers, and observing their evolution) is a consequence of the dynamics near the ‘saddle’, where mixing between two adjacent vortices appears to take place. These islands around the separatrices are commonly found in non-integrable Hamiltonian systems, and here they serve as implication of chaotic mixing. Results from the particle analysis further confirm that chaotic mixing is a consequence of the temporal behavior of the amplitude associated with the global background flow. Even though we have assumed much simpler temporal behavior for the amplitude in our simulations, the super-diffusion found in the simpler cases affirms that chaotic mixing should be expected as a result of the instability of the shear flow coupled to the gravity surface waves. This may imply that the entrainment rate of humidity into air could be enhanced by the coupling of weak wind with surface waves.

The calculations presented here will serve as a useful constraint for future numerical simulations of wind-driven interface instabilities. Thus, paradoxically, while tests of numerics involving the linear behavior of such systems can be done, they are challenging to apply; in contrast, it should be relatively easy to test the numerics in the weakly nonlinear limit.

This work was supported in part by the DOE-funded ASCI/Alliances Center for Thermonuclear Flashes at the University of Chicago. We thank N.J. Balmforth, N.R. Lebovitz and S.C. Venkataramani for helpful conversations. YNY acknowledges support from NASA and Northwestern University, and computation support from Argonne National Labs.

## Appendix

### A. Large $G$ behavior

We are interested in cases for which the factor  $G$  is large. As already discussed, such cases not only correspond to the astrophysical limit of strong surface stratification, but also correspond to cases for which the growth rate of (linearly) unstable modes is small, i.e., to cases for which our analysis is actually appropriate.

In order to proceed, we need to adopt a specific wind profile; in what follows, we will use a profile of the form  $U = U_{max}(1 - e^{-y})$ . However, we note that our basic results hold for more general wind profiles. From equation 3.6 we know that the unstable modes will have to be of the same order as  $G$ , and therefore  $K \gg 1$ ; this allows us to write a WKB expansion for the solution of the perturbation stream function of equation (3.1) for the wind. The equation we have to solve for large  $K$  is therefore

$$\phi_{,yy} - \left[ K^2 + \frac{U_{,yy}}{U - C} \right] \phi = 0; \quad (\text{A1})$$

by rescaling  $y \rightarrow Ky$ , we have

$$\phi_{,yy} - \left[ 1 + \frac{1}{K^2} \frac{U_{,y/K,y/K}}{U - C} \right] \phi = 0 \quad (\text{A2})$$

or

$$\phi_{,yy} - F(y/K)\phi = 0, \quad (\text{A3})$$

where  $F$  is a slowly varying function of its argument, as illustrated in figure A1. The boundary condition at the interface is:

$$KC^2 - r[KC^2\phi_y|_o - CU'|_o] - G(1 - r) = 0. \quad (\text{A4})$$

From figure A1 it is obvious that the WKB approximation will break down at two

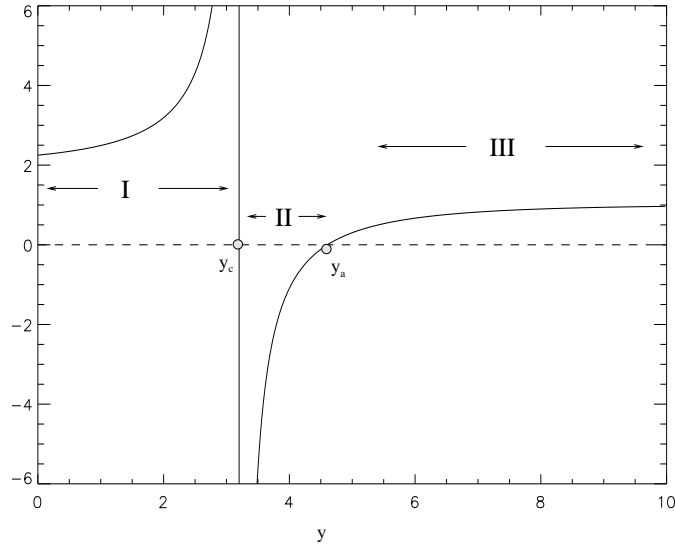


FIGURE A1. The function  $F$ .

points: The first one is at  $y = y_c$ , where the critical layer is located (and where  $F$  becomes singular); the second one is at  $y = y_a$ , where  $F = 0$ . For this reason, we will

have to decompose the  $y$ -axis into three regions: I.  $0 < y < y_c$ ; II.  $y_c < y < y_a$ ; III.  $y_a < y$ . The first-order solutions of the WKBJ equations therefore are:

$$(I) \quad \phi = A_1 \frac{1}{\sqrt{w}} e^{-\int_0^y w dy'} + B_1 \frac{1}{\sqrt{w}} e^{+\int_0^y w dy'}, \quad (A5)$$

$$(II) \quad \phi = A_2 \frac{1}{\sqrt{w}} \sin\left(\int_{y_c}^y w dy' - \pi/4\right) + B_2 \frac{1}{\sqrt{w}} \cos\left(\int_{y_c}^y w dy' - \pi/4\right), \quad (A6)$$

$$(III) \quad \phi = A_3 \frac{1}{\sqrt{w}} e^{-\int_{y_a}^y w dy'}, \quad (A7)$$

where

$$w(y) = \sqrt{\left|1 + \frac{1}{K^2} \frac{U_{,y/K, y/K i}}{U - C}\right|} = \sqrt{\left|1 + \frac{1}{K^2} \frac{e^{-y/K}}{1 - C - e^{-y/K}}\right|},$$

and the  $-\pi/4$  factor appearing in the solution for Region II is inserted for convenience, to be exploited shortly. The coefficients  $A_1, B_1, A_2, B_2, A_3$  are connected through the solutions at the points where the WKBJ approximation breaks down, and can be obtained using matched asymptotics. Thus, close to  $y = y_a$  it is well-known that the solution is an Airy function; the consequent connection formulae are given below (Olver 1997). For  $y < y_a$ ,

$$\begin{aligned} \phi &= \frac{2A_3}{\sqrt{w}} \sin\left[-\int_{y_a}^y w dy' + \pi/4\right], \\ &= \frac{2A_3}{\sqrt{w}} \left\{ \sin[I_1] \cos\left[\int_{y_c}^y w dy' - \pi/4\right] - \cos[I_1] \sin\left[\int_{y_c}^y w dy' - \pi/4\right] \right\}, \end{aligned}$$

and therefore

$$B_2 = 2A_3 \sin[I_1], \quad A_2 = -2A_3 \cos[I_1], \quad (A8)$$

where  $I_1 = \int_{y_c}^{y_a} w dy'$ . The solutions near the critical point  $y = y_c$  satisfy the equation

$$\phi_{,yy} - \frac{U_c''}{K U_c' y} \phi = 0 \quad (A9)$$

The solutions of the above equations are given in terms of  $z = -(y - y_c)U_c''/U_c'K > 0$  by

$$f_1(z) = \sqrt{z} J_1(2\sqrt{z}), \quad f_2(z) = \sqrt{z} N_1(2\sqrt{z}), \quad (A10)$$

where  $J_1, N_1$  are, respectively, the first Bessel and Neumann (Bessel of the second kind) functions. The first terms in the asymptotic expansion for  $y \rightarrow +\infty$  are

$$f_1(z) \simeq \frac{\sqrt[4]{z}}{\sqrt{\pi}} \sin\left(2z^{1/2} - \pi/4\right), \quad f_2(z) \simeq -\frac{\sqrt[4]{z}}{\sqrt{\pi}} \cos\left(2z^{1/2} - \pi/4\right). \quad (A11)$$

Matching with the outer solution, we have

$$\phi = \sqrt{\pi} A_2 f_1(z) - \sqrt{\pi} B_2 f_2(z).$$

The asymptotic expansion for  $z \rightarrow 0^+$  is

$$f_1 \simeq z + \dots \quad (A12)$$

$$\pi f_2 \simeq -1 + z \ln|z| + \dots - (1 - 2\gamma)z + \dots, \quad (A13)$$

where  $\gamma$  is the Euler-Masceroni constant. Thus, we can identify  $f_1$  with the regular Frobenius solution  $\phi_a$ , and  $f_2$  with the singular Frobenius solution  $\phi_b$ . Here we assumed that  $C_i$  is much smaller than  $G^{-1}$  (this is something that will be justified a posteriori).

For  $y < y_c$  the solutions of equation (A9) can be obtained by making the transformation

$z \rightarrow e^{-i\pi}z$  which is equivalent to taking the contour below the critical layer. By doing this the first Bessel function transforms to the first modified Bessel function that is growing exponentially and is real while the second one transforms to a linear combination of an exponentially growing and an exponentially decreasing modified Bessel function, and due to the presence of the logarithm it is going to have an imaginary part. Their asymptotic expansion for  $y \rightarrow \infty$  is

$$f_1 \simeq -\frac{\sqrt[4]{z}}{2\sqrt{\pi}}e^{+2\sqrt{z}}, \quad f_2 \simeq \frac{\sqrt[4]{z}}{2\sqrt{\pi}} \left[ ie^{2\sqrt{z}} - e^{-2\sqrt{z}} \right], \quad (\text{A14})$$

with  $z = (y - y_c)U_c''/U_c'K > 0$ . The inner solution for negative large  $z$  can be then written as

$$\phi_{in} = \sqrt{\pi}(A_2f_1 - B_2f_2), \quad (\text{A15})$$

$$= -\frac{\sqrt[4]{z}}{2} \left[ (A_2 + iB_2)e^{2\sqrt{z}} - B_2e^{-2\sqrt{z}} \right]. \quad (\text{A16})$$

Matching with the outer solution then gives

$$\phi = \frac{1}{2\sqrt{w}} \left[ -(A_2 + iB_2)e^{-\int_{y_c}^y w dy'} + B_2e^{+\int_{y_c}^y w dy'} \right] \quad (\text{A17})$$

or

$$\phi = -\frac{A_2 + iB_2}{2}e^{I_2} \frac{1}{\sqrt{w}}e^{-\int_0^y w dy'} + \frac{B_2}{2}e^{-I_2} \frac{1}{\sqrt{w}}e^{\int_0^y w dy'}, \quad (\text{A18})$$

where  $I_2 = \int_0^{y_c} w dy'$ . Gathering all the terms then gives

$$A_1 = A_3 \left( \cos[I_1] - i \sin[I_1] \right) e^{+I_2}, \quad B_1 = A_3 \sin[I_1] e^{-I_2}, \quad (\text{A19})$$

and

$$\phi = A_3 \left[ \sin(I_1)e^{-I_2}e^{+\int_0^y w dy'} + \cos(I_1)e^{+I_2}e^{-\int_0^y w dy'} - i \sin(I_1)e^{+I_2}e^{+\int_0^y w dy'} \right]. \quad (\text{A20})$$

The values of  $\phi$  and  $\phi_{,y}$  at zero are therefore

$$\phi|_0 = A_3 \left[ \sin(I_1)e^{-I_2} + \cos(I_1)e^{+I_2} - i \sin(I_1)e^{+I_2} \right], \quad (\text{A21})$$

$$\phi_{,y}|_0 = A_3 \left[ \sin(I_1)e^{-I_2} - \cos(I_1)e^{+I_2} + i \sin(I_1)e^{+I_2} \right], \quad (\text{A22})$$

where we have kept terms only to first order in  $K$ . For the given wind profile  $(1 - e^{-x})$ , we have:

$$y_c = -K \ln(1 - C), \quad y_a = -[K \ln(1 - C) - K \ln(1 + 1/K^2)],$$

$$I_1 \simeq \frac{\pi}{2K} + \mathcal{O}(1/K^3), \quad (\text{A23})$$

$$I_2 \simeq y_c + \mathcal{O}(1/K^2) = -K \ln(1 - C) + \mathcal{O}(1/K), \quad (\text{A24})$$

$$\sin(I_1) \simeq \frac{\pi}{2K}, \quad \cos(I_1) \simeq 1, \quad e^{-I_2} = (1 - C)^K.$$

Normalizing so that  $\phi|_0 = 1$ , we then obtain

$$\phi_{,y} = \frac{\sin(I_1)e^{-I_2} - \cos(I_1)e^{+I_2} + i \sin(I_1)e^{+I_2}}{\sin(I_1)e^{-I_2} + \cos(I_1)e^{+I_2} - i \sin(I_1)e^{+I_2}}, \quad (\text{A25})$$

or

$$\phi_{,y} = -1 + \frac{2 \sin(I_1) e^{-I_2}}{\sin(I_1) e^{-I_2} + \cos(I_1) e^{+I_2} - i \sin(I_1) e^{+I_2}}. \quad (\text{A26})$$

The second term in equation (A26) is exponentially small when compared to 1 since  $I_2 \sim K$ ; neglecting this term when appropriate then allows  $\phi_{,y}$  to be written as

$$\phi_{,y} = -1 + 2i \sin^2(I_1) e^{-2I_2}, \quad (\text{A27})$$

where we have kept only the first term in the expansion of the real and imaginary parts. Plugging in this value of  $\phi_{,y}$  in equation (A4), we obtain, to zeroth order,

$$C_0 = \sqrt{\frac{1-r}{1+r} \frac{G}{K}} = \sqrt{\mathcal{A}_t G / K}, \quad (\text{A28})$$

which corresponds to the gravity wave in the absence of a wind;  $\mathcal{A}_t$  is the Atwood number. For our purposes, this is as far as we need to go in analyzing the real part of  $C$ .

We next turn to analyzing the imaginary part of  $C$ . To obtain the first order in  $\text{Im}\{C\} = C_i \ll C_0$  we have:

$$2K(1-r)C_0C_i - rKC_0^2(1 + \phi_{,y}) = 0, \quad C_i = \frac{1}{2} \frac{r}{1-r} C_0(1 + \phi_{,y}), \quad (\text{A29})$$

so that

$$C_i = \frac{rC_0}{1-r} \sin^2(I_1) e^{-2I_2}, \quad (\text{A30})$$

$$\text{Im}\{C_1\} = \frac{r\pi^2}{4(1-r)} \frac{1}{\mathcal{A}_t^2 G^2} \left(\frac{\mathcal{A}_t G}{K}\right)^{5/2} \left[ \left(1 - \frac{1}{\sqrt{K/(\mathcal{A}_t G)}}\right)^{(K/\mathcal{A}_t G)} \right]^{2\mathcal{A}_t G}. \quad (\text{A31})$$

We note that  $(1 - 1/\sqrt{x})^{2x}$  is a bounded function smaller than one, and therefore  $C_i$  has a negative exponential dependence on  $G$ . We note further that this exponential dependence should be independent of the wind profile, and in a more general case — for which  $U(y)$  is the wind profile and  $U^{-1}(c)$  is its inverse — the growth rate will be proportional to  $C_i \sim \exp[-2KU^{-1}(c)]$ ; this can be re-written as  $C_i \sim f(c(K))^{\mathcal{A}_t G}$ , with  $f(c) \equiv \exp[-2U^{-1}(C)/C]$  a bounded function and  $C = C_0$ . The interpretation of equation (A30) is straightforward: it simply states that the growth rate is proportional to the negative exponential of the height of the critical layer, as measured in units of the wavelength.

## REFERENCES

- ALEXAKIS, A., YOUNG, Y.N. & ROSNER, R. 2002 Shear instability of fluid interfaces: Stability analysis. *Phys. Rev. E* **65**, 026313.
- BALMFORTH, N.J. & PICCOLO, C. 2001 The onset of meandering in a barotropic jet. *J. Fluid Mech.* **449**, 85–114.
- BENNEY, D.J. & BERGON, F.R.JR 1969 A new class of nonlinear waves in parallel flows. *Stud. Appl. Math.* **48**, 181.
- BENNEY, D.J. & MASLOWE, S.A. 1975 The evolution in space and time of nonlinear waves in parallel shear flows. *Stud. Appl. Math.* **54**, 181.
- VENKATARAMANI, C., ANTONSEN, T.M. & OTT, E. 1998 Anomalous diffusion in bounded temporally irregular flows. *Physica D* **112**, 412–440.
- CHANDRASEKHAR, S. 1961 *Hydrodynamic and Hydromagnetic Stability*. Oxford: Clarendon.

- CHURILOV, S.M. & SHUKMAN, I.G. 1987 Nonlinear stability of stratified shear flow: viscous critical layer. *J. Fluid Mech.* **180**, 1.
- CHURILOV, S.M. & SHUKMAN, I.G. 1988 Nonlinear stability of a stratified shear flow in the regime with an unsteady critical layer. *J. Fluid Mech.* **194**, 187.
- CHURILOV, S.M. & SHUKMAN, I.G. 1996 The nonlinear critical layer resulting from the spatial or temporal evolution of weakly unstable disturbances in shear flows. *J. Fluid Mech.* **318**, 189.
- DRAZIN, P.G. 1970 Kelvin-Helmholtz instability of finite amplitude. *J. Fluid Mech.* **42**, 321.
- DRAZIN, P.G. & REID, W.H. 1981 *Hydrodynamic Stability*. Cambridge University Press.
- BOFFETTA, G., LACORATA, G., REDAELLI, G. & VULPIANI, A. 2001 Detecting barriers to transport: a review of different techniques. *Physica D* **159**, 58–70.
- GOLDSTEIN, M.E. & HULTGEN, L.S. 1988 Nonlinear spatial evolution of an externally excited instability wave in a free shear layer. *J. Fluid mech.* **197**, 295.
- HABERMAN, R. 1972 Critical layers in parallel flows. *Stud. Appl. Math.* **51**, 139.
- LATINI, M. & BERNOFF, A.J. 2001 Transient anomalous diffusion in poiseuille flow. *J. Fluid Mech.* **441**, 399–411.
- MILES, J. 1957 On the generation of surface waves by shear flows. *J. Fluid Mech.* **3**, 185.
- MILES, J. 1959 On the generation of surface waves by shear flows. Part 2. *a J. Fluid Mech.* **6**, 568.
- MILES, J. 1959 On the generation of surface waves by shear flows. Part3. Kelvin-Helmholtz instability *b J. Fluid Mech.* **6**, 583.
- MILES, J. 1962 On the generation of surface waves by shear flows. Part 4. *J. Fluid Mech.* **13**, 433.
- MILES, J. 1967 On the generation of surface waves by shear flows. Part 5. *J. Fluid Mech.* **30**, 163.
- MILES, J. 1999 Wind-to-wave energy transfer. In *Wind-over-wave couplings: perspective and prospects* (ed. N. T. S.G. Sajjadi & J. Hunt). Oxford: Clarendon.
- OLVER, F.W.J. 1997 *Asymptotics and special functions*. A K Peters, Natick Massachusetts.
- ROSNER, R., ALEXAKIS, A., YOUNG Y.N. & TRURAN, J.W., HILLEBRANDT, H. 2001 On the c/o enrichment of nova ejecta. *Astrophysical Journal* **526**, L177–L179.
- WARN, T. & WARN, H. 1978 The evolution of a nonlinear critical level. *Stud. Appl. Math.* **59**, 37–71.